A Szilikátipari Tudományos Egyesület lapja

építőanyag

Journal of Silicate Based and Composite Materials

A TARTALOMBÓL:

- Comparison of sorption properties of natural and synthetic takovites, $Ni_6Al_2(OH)_{16}CO_3.4H_2O$
- Studies on the spatial variability of rebound hammer test results recorded at in-situ testing
- Measurable properties of Al_2O_3 ceramic Injection Molding Raw Materials
- Experiments on the buckling behaviour of glass columns. Part 2.
- Simple basic model for concrete and its application. Part 3.

2013/4

Sustainable Development with Concrete

Concrete Thinking for a sustainable world

PCA Portland Cement Association

The Portland Cement Association (PCA, http://www.cement.org) is a powerful and vocal advocate for sustainability, jobs creation, economic growth, infrastructure investment, and overall innovation and excellence in construction.

The Concrete Thinker website is a resource to help design professionals make sustainable design a reality through the durability, versatility and energy performance of concrete.

Through application overviews, case studies and other resources and tools learn how forward-thinking architects rely on concrete to create healthy and vibrant places to work, live and play for years to come.

The Concrete Thinker website was developed by the Portland Cement Association (PCA) to demonstrate how concrete can be used to achieve sustainable solutions.

A wide variety of concrete methods and products give you the techniques to create both beauty and function in ways that improve the impact of buildings on the environment.
Sustainable development is about balancing human needs with the earth's capacity to meet them. Concrete offers a wide range of capabilities to help achieve this balance.

Explore the site. Get inspired. Share your ideas. Be a Concrete Thinker.
http://www.concretethinker.com

építőanyag

Journal of Silicate Based and Composite Materials

2013/4

TARTALOM

97 Természetes és szintetikus takovitok, $Ni_6Al_2(OH)_{16}CO_3.4H_2O$ szorpciós tulajdonságainak összehasonlítása

Eleonora BUTENKO ▪ David BISH ▪ Galina ABROSIMOVA ▪ Alexey KAPUSTIN

102 Mérőhelyek közötti változékonyság értékelése Schmidt-kalapáccsal végzett helyszíni vizsgálat során

Katalin SZILÁGYI ▪ Adorján BOROSNYÓI

107 Al_2O_3 kerámia fröccsöntés alapanyagának vizsgálatai

EGÉSZ Ádám ▪ GÖMZE A. László

112 Üvegoszlopok kihajlásának laboratóriumi vizsgálata

NEHME Kinga ▪ JAKAB András ▪ Salem Georges NEHME

118 Betonkeverékek egyszerűsített alapmodellje és alkalmazása

PEKÁR Gyula

127 Egyesületi és szakhírek

CONTENT

97 Comparison of sorption properties of natural and synthetic takovites, $Ni_6Al_2(OH)_{16}CO_3.4H_2O$

Eleonora BUTENKO ▪ David BISH ▪ Galina ABROSIMOVA ▪ Alexey KAPUSTIN

102 Studies on the spatial variability of rebound hammer test results recorded at in-situ testing

Adorján BOROSNYÓI ▪ Katalin SZILÁGYI

107 Measurable properties of Al_2O_3 ceramic injection molding raw materials

Ádám EGÉSZ ▪ László A. GÖMZE

112 Experiments on the buckling behaviour of glass columns

Kinga NEHME ▪ András JAKAB ▪ Salem Georges NEHME

118 Simple basic model for concrete and its application

Gyula PEKÁR

127 Society and professional news

A finomkerámia-, üveg-, cement-, mész-, beton-, tégla- és cserép-, kő- és kavics-, tűzállóanyag-, szigetelőanyag-iparágak szakmai lapja
Scientific journal of ceramics, glass, cement, concrete, clay products, stone and gravel, insulating and fireproof materials and composites

A folyóiratot referálja:
Cambridge Scientific Abstracts, ProQuest.
A szakmai rovatokban lektorált cikkek jelennek meg.
Kiadja a Szilikátipari Tudományos Egyesület
1034 Budapest, Bécsi út 122–124.
Telefon és fax: +36-1/201-9360
E-mail: epitoanyag@szte.org.hu
Felelős kiadó: ASZTALOS István SZTE elnök
Tördelő szerkesztő: NÉMETH Hajnalka

Címlapfotó/Cover photo by KÓSA Luca Kornélia

Egy szám ára: 1250 Ft
A lap az SZTE tagok számára ingyenes.

Belföldi terjesztés: SZTE
Külföldi terjesztés: Batthyany Kultur-Press Kft.

Online ISSN: 2064-4477 ▪ Print ISSN: 0013-970x
INDEX: 2 52 50 ▪ 65 (2013) 97–128

65. évf. 4. szám

Comparison of sorption properties of natural and synthetic takovites, $Ni_6Al_2(OH)_{16}CO_3 \cdot 4H_2O$

Eleonora BUTENKO ▪ Azov Sea State Technical University, University Street 7, 87500 Mariupol, Ukraine ▪ e-mail: butenkoeo@rambler.ru

David BISH ▪ Indiana University, 1001E. 10th Street, Bloomington, IN 47405 USA ▪ e-mail: bish@indiana.edu

Galina ABROSIMOVA ▪ Institute of Solid State Physics RAS, 142432 Chernogolovka, Russia ▪ e-mail: gea@issp.ac.ru

Alexey KAPUSTIN ▪ Azov Sea State Technical University, University Street 7, 87500 Mariupol, Ukraine ▪ e-mail: kapustin_a_e@pstu.edu

Received: 16. 12. 2013. ▪ Érkezett: 2013. 12. 16. ▪ http://dx.doi.org/10.14382/epitoanyag-jsbcm.2013.18

Abstract

Most clay minerals are cation exchangers, but the layered double hydroxides are unique in having anion-exchange properties. Takovite, $Ni_6Al_2(OH)_{16}CO_3 \cdot 4H_2O$, is a layered double hydroxide that occurs in low-silica weathering environments. Natural and synthetic specimens of takovites were compared using atomic absorption spectroscopy, X-ray powder diffraction, and titration with Hammett indicators. In addition, the sorption of alcoholate-anions was compared and the kinetics of chromate and naphthalene sorption were evaluated. The natural and synthetic specimens of takovite have identical structures, chemical properties, and selectivities for organic and inorganic ions. However, the measured rates of physisorption and anion exchange were distinct, possibly due to variations in crystallite size and shape, leading to different access to internal active sites.

Keywords: clay minerals, takovite, sorption

Eleonora Butenko

Works at the Department of Chemical Technology and Engineering, Azov Sea State Technical University. She had BSc in chemistry (2006) and MSc in analytical chemistry (2007) at Donetsk National University, Chemistry Faculty. She had a technician practice at Steel work "Azovstal" (2006). She was technician and later graduate student at Department of Chemical Technology and Engineering, Azov Sea State Technical University (2007). Main fields of interests: processes of physical sorption and anion-exchange of organic compounds on LDHs to solve environmental problems.

David Bish

BSc (1974), Furman University, PhD (1977), Pennsylvania State University, Postdoctoral fellow (1977-1980), Harvard University. Haydn Murray Chair of Applied Clay Mineralogy, Department of Geological Sciences, Indiana University. Main fields of interests: application of crystal chemical and crystal structural fundamentals to geological, materials, and environmental problems, surface properties of smectites, behavior of fluorine in brick raw materials.

Galina Abrosimova

PhD, Scientific Secretary of the Russian Academy of Sciences Institute of Solid State Physics Laboratory of Structure Research. Main fields of interests: solid state physics, experimental physics, nanomaterials, crystal engineering.

Alexey Kapustin

Doctor of Science (chemistry). Graduated at Moscow Mendeleev Chemical Technological Institute (1975–1981). His PhD thesis was "Alcohol Ethoxylation Reactions" (1983). His DSc thesis was "Creation of Basic Heterogeneous Catalysts" (1996). Works at Azov Sea State Technical University. Head of Department of Chemical Technology and Engineering of Azov Sea State Technical University, Mariupol, Ukraine.

1. Introduction

Clay minerals are the most widespread natural inorganic ion-exchangers on the surface of the Earth [1,2,3]. Most clay minerals are solid acids, although some, including the layered double hydroxides, have a basic character. Unlike most clay minerals that have a permanent negative charge, making them cation exchangers, the layered double hydroxides have a permanent positive charge, making them anion exchangers. The mineral takovite ($Ni_6Al_2(OH)_{16}CO_3 \cdot 4H_2O$), a layered double hydroxide based on the brucite structure, is an important nickel-containing phase in low-silica weathering deposits. Takovite occurs in karstic bauxites and with minerals such as nepouite, gaspeite, and carrboydite in weathered nickel sulfide deposits [4,5].

Takovite and related minerals in the pyroaurite group have structures in which brucite-like layers carry a net positive charge due to the isomorphous substitution of trivalent for divalent cations (such as Al^{+3}-for-Ni^{+2} in takovite). Carbonate anions and H_2O molecules occupy the interlayer region. Previous experiments have shown that acid treatments do not result in destruction of the structure and instead result in anion exchange [5].

The synthetic analogs of takovite, pyroaurite, and hydrotalcite are active heterogeneous catalysts in basic catalytic processes, such as oxialkylation, aldol condensations, etc. [6]. In addition, the naturally occurring anionic clay minerals and their synthetic analogs are widely used as sorbents, catalysts, and catalyst precursors. The compositions of the natural and synthetic materials can be identical, and their chemical and physical properties, including their sorption and catalytic properties, can also be identical. However, substantial differences often exist between the properties of the natural and synthetic layered double hydroxides resulting from compositional and structural heterogeneities related to their modes of origin (natural vs. synthesized). The most important difference between the natural anionic minerals and their synthetic analogs is that the natural anionic clays typically display selectivity towards chiral isomers [7]. Such differences in chiroptical selectivity would not be expected on the basis of our knowledge of the crystal structures of these materials.

2. Experimental

To compare the structure, physical-chemical properties, and catalytic activity of natural takovite with its synthetic analog, the latter was obtained by precipitation. This method involved mixing a concentrated (1 M), aqueous solution of Ni^{2+} and Al^{3+} nitrate with aqueous sodium hydroxide-carbonate to yield an amorphous gel. At a final pH of 9-10, the carbonate concentration exceeded the stoichiometric requirements for takovite formation by a factor of approximately three. Following precipitation, the gel was allowed to crystallize in the liquid phase by heating for 24 h at 65 °C and was then dried at 125 °C.

Synthetic takovite was characterized by atomic absorption spectroscopy (Saturn-4 atomic absorption spectrophotometer

with flame atomizer), X-ray powder diffraction (XRD), and titration with Hammett indicators. Confirmation of the structural state of the synthetic materials was done by XRD using a Bruker D8 diffractometer with Cu Kα radiation and a SolX solid-state detector. In order to investigate the basic properties of natural and synthetic takovites, titration with Hammett indicators was used [8]. A sample of takovite in a small beaker filled with benzene was stirred on a magnetic stirrer. Subsequently, a glass cylinder, divided by a porous separator on which a standard sample was installed was inserted into the beaker. A Hammett indicator was added to the benzene and changes in color were observed on the surface of the standard sample. The following indicators were used: Bromothymol Blue (pK_a = 7.2), 4-Chlor-2-nitroanilin (pK_a = 17.2), 4-Chloranilin (pK_a = 26.5), purchased from Aldrich, and 2,4,6-Trinitroanilin (pK_a = 12.2), 2,4-Dinitroaniline (pK_a = 15.0), and 4-Nitroanilin (pK_a = 18.4), all purchased from Fluka. Because the takovites have a blue-green color, a sample of calcined MgO was used for comparison.

The sorption selectivity of synthetic and natural takovites for different alcoholate-ions was measured using a solution containing the respective sodium alcoholates. Deionized water was used and measurements were done under a nitrogen atmosphere. The total concentration of alcoholates corresponded to the concentration of basic sites in takovites, determined by indicator titration (E = 0.8 meq/g). A solution in which takovite was suspended was placed on a stirrer and maintained at room temperature for 24 hours. The concentration of remaining alcoholates was then determined using a Chrome-5 chromatograph.

The kinetics of chromate adsorption was determined using a solution of 0.017 mol/l K_2CrO_4 to which takovite was added in a retort. The solution was mixed on a magnetic mixer and aliquots of the solution were sampled at different intervals (1, 3, 10 min., etc.). This solution was filtered and CCl_3COOH and a 0.5 % solution of diphenylcarbazide was added and stirred for 10 min. The absorbance of the solution was then measured at 546.1 nm using a KFK-3 photocolorimeter. Finally, the sorption of naphthalene was evaluated with a Chrome-5 chromatograph by measuring the concentration of naphthalene remaining in solution after introduction of takovite.

3. Results and discussion

Atomic absorption chemical analyses showed the followed composition for the synthetic takovite: Al – 7.58 mol %; NiO – 16.40 %; C – 9.47 mol %; O – 66.55 %. The corresponding structural formula based on these chemical analyses is approximately $[Ni_2Al(OH)_6]CO_3$.

The XRD pattern of synthetic takovite in Fig. 1 is consistent with the three-layer rhombohedral structure, with R-3m space group and unit-cell parameters: a = 3.025 Å, c = 22.595 Å. The positions of the reflections corresponding to a natural takovite are indicated by red lines in the figure, and weak reflections (101 – 43.6°, 104 – 48.08°, 1 0 10 – 68.92°, 0 1 11 – 73.52°, 1 0 13 – 83.94°) were not resolved due to the large peak widths. XRD analysis gave a d_{001} of ~7.6 Å for both synthetic and natural takovites.

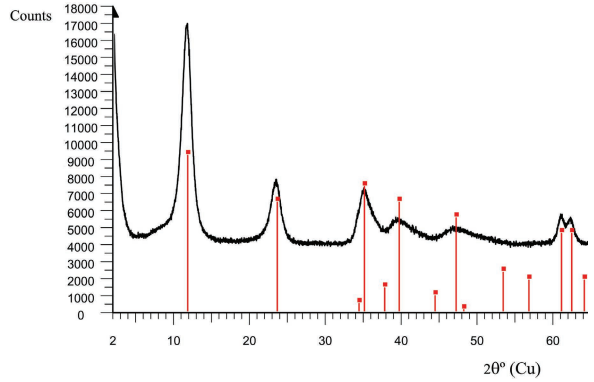

Fig. 1. XRD pattern of synthetic takovite, showing the comparison with ICDD data 15-0087 for a natural takovite (vertical red lines)
1. ábra Szintetikus takovit röntgendiffraktogramja, összehasonlítva az ICDD 15-0087 adatbázisban szereplő természetes takovitéval (függőleges vörös vonalak)

H_0	$H_0 > 7.2$	$H_0 > 9.3$	$H_0 > 12.2$
Natural	0.79	0.30	0.01
Synthetic	0.82	0.27	≤ 0.01

Table 1. Concentration of basic sites of different strength on natural and synthetic takovites
1. táblázat A természetes és szintetikus takovitok egyes csoportjainak koncentrációja

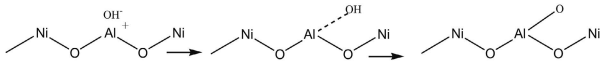

Fig. 2. Transformation of the basic layer structure [6]
2. ábra A rétegszerkezet átalakulása [6]

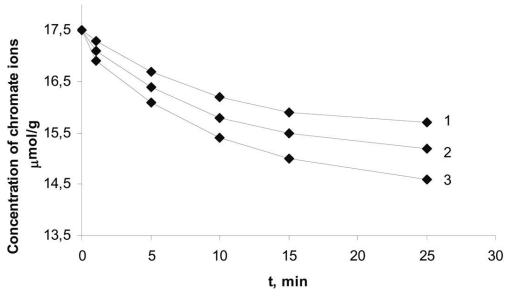

Fig. 3. Adsorption of chromate anions as a function of time for different amounts of natural takovite in suspension (1 – 0.05 g; 2 – 0.07 g; 3 – 0.1 g)
3. ábra Kromát anionok adszorpciójának időbeli alakulása különböző összetételű természetes takovit szuszpenziókban (1 – 0.05 g; 2 – 0.07 g; 3 – 0.1 g).

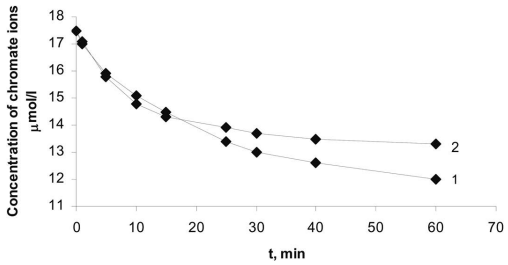

Fig. 4. Sorption of chromate onto synthetic and natural takovite as a function of time (1 – natural takovite; 2 – synthetic takovite)
4. ábra Kromát szorpciójának időbeli alakulása természetes és szintetikus takovit esetén (1 – természetes takovit; 2 – szintetikus takovit)

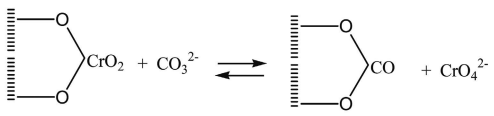

$CO_3^{2-} > NO_3^- > CrO_4^{2-} > SO_4^{2-} > HVO_4^{2-} > OH^- > Cl^- > MnO_4^-$

Fig. 5. The order of preference of synthetic and natural takovites for anions [1]
5. ábra Anionok reakcióképességének sorrendje természetes és szintetikus takovit esetén [1]

T, °C	100		200		300		400		500		600	
	B	L	B	L	B	L	B	L	B	L	B	L
Natural	0.79	nd	0.45	0.15	0.30	0.19	0.08	0.17	0.04	0.17	nd	0.10
Synthetic	0.82	nd	0.55	0.01	0.31	0.14	0.13	0.22	0.03	0.20	nd	0.12

Table 2. The concentration of basic sites of takovites, mmol/g (B – Bronsted, L – Lewis sites; 12.2 < H_0 < 17.2, nd – not detected)
2. táblázat A takovitok egyes csoportjainak koncentrációja, mmol/g (B – Bronsted, L – Lewis; 12.2 < H_0 < 17.2, nd – nem érzékelhető)

Determination of the acid-base properties of takovites using Hammett indicators of different pK_a gave the following strength distribution of basic sites (*Table 1*). These results show that the number of basic sites in synthetic takovite is comparable to that in the natural sample, and the distribution of the strength of basic sites in natural and synthetic takovite is also essentially identical.

Calcining layered double hydroxides causes transformation of the basic layer structure due to dehydration and then dehydroxylation, changing the total basicity and redistributing basic sites on the surface as shown in *Fig. 2* [6].

Calcining of takovites at various temperatures up to 600°C resulted in the transformation of Bronsted basic sites into Lewis sites (*Table 1*), which was accompanied by reduction of the total number of sites with a simultaneous increase in the strength of the basic sites, as quantified in *Table 2*.

Adsorption of chromium anions by synthetic and natural takovite was investigated to understand the anion sorption behavior of these materials. Results of chromate adsorption kinetics experiments for natural takovite are shown in *Fig. 3*, showing that the rate of adsorption is proportional to the amount of takovite in suspension (and directly proportional to the concentration of chromate anions in solution). Similar results were obtained for synthetic takovite.

Knowing the concentration of basic sites in takovite (E in mmol/g) and the amount of adsorbent, it is possible to calculate the concentration of basic sites in the reaction mixture. As the concentrations of basic sites in synthetic and natural takovites are essentially identical, we anticipated that the sorption processes in these materials would be identical. But *Fig. 4* shows that sorption onto synthetic takovite was initially more rapid than onto natural takovite, with natural takovite ultimately taking up more chromate ions. The initial behavior is in agreement with expectations that sorption will be more rapid onto the very fine-grained synthetic takovite. The behavior after about 20 minutes may be related to a larger intrinsic exchange capacity for the natural material.

After completion of the sorption process, the takovites were washed with deionized water and held in water for 48 hours without access to air under a nitrogen atmosphere. Analysis of the liquid phase revealed the absence of chromium ions, demonstrating that desorption did not take place. However, when the takovites were placed in a carbonate-bearing solution, chromate anions were detected, demonstrating the occurrence of anion exchange via the following process:

As previously demonstrated, treatments with various dilute acids and salt solutions do not destroy the crystal structure of takovite. The order of preference of synthetic and natural takovites for anions was obtained from anion-exchange experiments, and natural takovites showed pronounced preference for carbonate-ions over other anions [5], which is also true for other minerals of the pyroaurite and hydrotalcite groups, see *Fig. 5* [1].

In order to differentiate between anion-exchange and physisorption in the adsorption of alcoholate-ions, we conducted additional experiments using alcoholate ions. After conclusion of the sorption process, the takovite powder was extracted from solution, washed in deionized water, dried, and placed in a 1 % aqueous NaOH solution. Chromatographic analysis of these solutions revealed the presence of alcoholate ions.

The data in *Table 3* suggest that the ability of takovite to sorb alcoholate anions diminishes with an increase in the molecular weight of the hydrocarbon radical. This behavior may be explained by an orientation of the hydrocarbon radicals parallel to the basal layers, thereby blocking nearby basic sites. If they were oriented perpendicular to the basal layers, the sorption behavior of all alcoholate ions should be approximately identical. In addition the latter case would lead to an increase in the basal spacing which was not observed.

Anions	CH_3O^-	$C_2H_5O^-$	$C_3H_7O^-$	$C_4H_9O^-$	$C_7H_{15}O^-$	$C_7H_{15}O^-$	$C_{12}H_{25}O^-$
Natural	100	66	37	19	4	1	< 0.1
Synthetic	100	70	41	23	8	1	–

Table 3. Selectivity of takovites to alcoholate ions (relative units)
3. táblázat Takovitok alkoholát ion szelekciója (relatív mérték)

X-ray diffraction study revealed that ion-exchange of takovites with nitrate and chloride anions caused only minor changes in the structure with increases in basal spacing [5]. However ion-exchange with sulfate, chromate, and vanadate anions led to considerable change in the basic structure and to formation of two different structures (*Table 4*).

Anion	CO_3^{2-}	SO_4^{2-}	CrO_4^{2-}	HVO_4^{2-}
d_{001} (Å)	7.95	8.25	8.29	8.97

Table 4. Basal spacing of takovite with different interlayer anions
4. táblázat Takovitok bázistávolsága különböző rétegközi anionok esetén

It is interesting to compare the above results for chromate adsorption with the results for absorption of aromatic hydrocarbons of naphthalene by natural and synthetic takovites (*Fig. 6*).

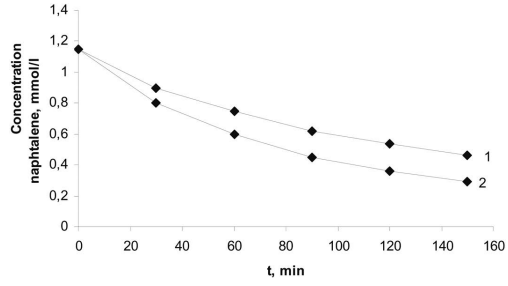

Fig. 6. Sorption of naphthalene on synthetic and natural takovites as a function time (1 – synthetic takovite; 2 – natural takovite)
6. ábra Naftalén szorpciójának időbeli alakulása természetes és szintetikus takovit esetén (1 – szintetikus takovit; 2 –természetes takovit)

These aromatic hydrocarbons of naphthalene are contained in the interlayer as a result of cooperation of aromatic π-electrons with the electron orbitals and are physisorbed onto takovite, in contrast to sorption onto layered double hydroxides by anionic compounds such as naphthalene carboxylates or naphthalene nitrates [9,10]. The higher activity of natural takovite again is counter to what was expected and may result from the more-ordered layer structure and availability of active sites for the sorption of organic compounds.

The physisorption of naphthalene thus contrasts with the anion exchange of chromate, sulfate, and vanadate ions. Data in *Fig. 4* and *6* show that natural takovite has a greater capacity for anions and naphthalenes than does the synthetic takovite. These differences could reflect variations in crystal perfection as synthetic takovite is typically considerably more disordered than natural takovite [11]. However, one would normally expect more disordered material to be more effective at chemi- and physisorption than a well ordered material with larger crystallite size.

4. Conclusions

The results demonstrate that natural and synthetic takovites have similar compositions and structures, identical acid-basic properties, and identical selectivity series. Calcining of takovites transformed Bronsted basic sites into Lewis sites, accompanied by a reduction in the total number of sites and an increase in the strength of the basic sites. However, sorption of anions and naphthalenes occurs at different rates and with different degrees of absorption. It is likely that explanations for differences between the behavior of natural and synthetic takovites lie in differences in their crystallite sizes and degrees of structural order. XRD data demonstrate that the synthetic takovites have very small crystallite sizes and considerable strain, whereas natural takovite occurs in much larger crystallites with little strain. However, based on the XRD results, one would expect synthetic takovite to exhibit more-rapid adsorption kinetics and to have a larger exchange capacity, the opposite of our observations, possibly due to variations in crystallite size and shape, leading to different access to internal active sites.

References

[1] ASTM 15-0087. JCPDS – International Centre for Diffraction Data.

[2] Bish, D. L. – Brindley, G. W.: A re-investigation of takovite, a Ni-Al hydroxy-carbonate of the pyroaurite group. *American Mineralogist*, Vol. 62, 458-464. (1977)

[3] Bish, D.: Anion-exchange in takovite: applications to other minerals. *Bulletin de Mineralogie*, Vol. 103, 170-175. (1980)

[4] Duan, X. – Evans, D. G.: Layered Double Hydroxides. Structure and bonding. D.M.P. Mingos (Ed.). *Springer-Verlag.* Berlin. Heidelberg. (2006).

[5] Lebedeva, O. V. – Kapustin, A.E.: Problems of indicator titration of basic heterogeneous catalysts. *Ukrainian Chemical Journal*, Vol. 63, 25-27. (1997)

[6] Kapustin, A.: Inorganic anion-exchangers. *Russian Chemistry Reviews*, Vol. 60, 1398-1416. (1991)

[7] Kapustin, A.: Catalysis by layered double hydroxides. *Scientific problems of modern technology*, Vol. 16, 267-275. (2007)

[8] Kapustin, A.: Heterogeneous basic catalysis. Renata. Mariupol (in Russian) (2008)

[9] Putyera, K. – Bandosz, T. J. – Jagieo, J. – Schwarz, J. A.: Effect of template constraints on adsorption properties of synthetic carbons prepared within the gallery of layered double hydroxides. *Carbon*, Vol. 34, No. 12, 1996, pp. 1559–1567. http://dx.doi.org/10.1016/S0008-6223(96)00112-1 (1996)

[10] Radha, A. V. – Kamath, P. V. – Shivakumara, C.: Order and disorder among the layered double hydroxides: combined Rietveld and DIFFaX approach. *Acta Crystallographica Section B*, Vol. 63, No. 2, pp. 243-250. http://dx.doi.org/10.1107/S010876810700122X (2007)

[11] Vaccari, A.: Layered double hydroxides: present and future. V. Rives (Ed.). *Nova Science Publishers. Inc.* New York. (2002)

[12] Zhao, H. – Vance, G. F.: Molecular Inclusion Properties of Hydrophobic Organic Compounds by a Modified β-Cyclodextrin Intercalated within a Layered Double Hydroxide. *Journal of Inclusion Phenomena and Macrocyclic Chemistry*, Vol. 31, No. 4, August 1998, pp. 305-317. http://dx.doi.org/10.1023/A:1007965712719 (1998)

Ref.:
Eleonora **Butenko** – David **Bish** – Galina **Abrosimova** – Alexey **Kapustin**: *Comparison of sorption properties of natural and synthetic takovites, $Ni_6Al_2(OH)_{16}CO_3{\cdot}4H_2O$*
Építőanyag, 65. évf. 4. szám (2013), 97–101. p.
http://dx.doi.org/10.14382/epitoanyag-jsbcm.2013.18

Természetes és szintetikus takovitok, $Ni_6Al_2(OH)_{16}CO_3{\cdot}4H_2O$ szorpciós tulajdonságainak összehasonlítása

A legtöbb agyagásvány kationcserélő tulajdonsággal rendelkezik, azonban a réteges kettős hidroxidok különleges módon anioncserélő tulajdonságúak. A takovit $Ni_6Al_2(OH)_{16}CO_3{\cdot}4H_2O$ egy réteges kettős hidroxid, amely kis szilícium-tartalmú környezetben képződik. A cikkben természetes és szintetikus takovitok összehasonlítása történik atomabszorpciós spektroszkópiával, röntgendiffrakcióval és Hammett indikátoros titrálással. Ezen kívül, alkoholát anionok szorpciójának összehasonlítása, illetve kromátok és naftalének szorpciójának kinetikája is bemutatásra kerül. A természetes és szintetikus takovitoknak azonos a szerkezete, a kémiai jellemzői és a szerves és szervetlen ionszelekciója. Különbség mutatkozott a mért fiziszorpciós sebességben és az anioncserélésben, amely a kristályok eltérő méretéből és alakjából származhat, amely eltérő mértékében biztosít lehetőséget a belső aktív részek eléréséhez.

Kulcsszavak: agyagásványok, takovit, szorpció

Studies on the spatial variability of rebound hammer test results recorded at in-situ testing

Adorján BOROSNYÓI ▪ Assoc. Prof., BME, Dept. of Construction Materials and Engineering Geology ▪ adorjan.borosnyoi@gmail.com
Katalin SZILÁGYI ▪ PhD candidate, BME, Dept. of Construction Materials and Engineering Geology ▪ szilagyikt@gmail.com
Received: 14. 11. 2013. ▪ Érkezett: 2013. 11. 14. ▪ http://dx.doi.org/10.14382/epitoanyag-jsbcm.2013.19

Abstract
Variability of the in-situ rebound hammer tests is composed of the inherent variability of the measuring method and the spatial variability of the concrete performance properties. In-situ, Schmidt rebound hammer tests were performed at the bottom surface of a concrete slab, with dimensions of 25.0 m × 7.5 m. The studied region on was 22.0 m × 6.0 m. The analysis of the inherent variability of the rebound hammer tests was limited to the comparison of the statistical location parameters; mean, median and mode values. The spatial variability was analysed by contour plots and semivariograms of the statistical location parameters. It was demonstrated that the geostatistical methods may be applicable for the much smaller scale concrete structures than the scale of geological formations. Semivariograms and semivariogram models seem to be useful tools for the characterisation of spatial variability of concrete structures.
Keywords: concrete, rebound hardness, Schmidt hammer, spatial variability, statistical location parameters, semivariogram

Adorján Borosnyói
civil engineer (MSc), PhD, Associate Professor at BME Dept. of Construction Materials and Engineering Geology. Main fields of interest: cracking and deflection of reinforced concrete, application of non-metallic (FRP) reinforcements for concrete structures, bond in concrete, non-destructive testing of concrete, supplementary cementing materials for high performance concretes, concrete technology. Secretary of the fib Task Group 4.1 „Serviceability Models" and Chairman of the SZTE Concrete Division.

Katalin Szilágyi
civil engineer (MSc), PhD candidate at the Department of Construction Materials and Engineering Geology, Budapest University of Technology and Economics. Main fields of interest: diagnostics of concrete structures, non-destructive testing of concrete, concrete technology, shrinkage compensation of concretes. Member of the Hungarian Group of fib and the SZTE Concrete Division.

1. Introduction

The magnitude of the variation in the strength of structural concrete is a result of the level of quality control over the concrete production, transportation, compacting and curing procedures. The compressive strength of the concrete is not measured in the structure during in-situ non-destructive testing (NDT), but some other property is measured instead that is correlated to the compressive strength. The strength of concrete is estimated from a previously established relationship between the measured NDT property and the compressive strength. The uncertainty of the estimated compressive strength, therefore, depends both on the variability of the in-situ measurements and the uncertainty of the relationship between the measured NDT property and compressive strength. *Variability of the in-situ measurements* is composed of the *inherent variability* of the measuring method (repeatability and reproducibility; attributed to the operation mode and the calibration conditions of the testing device, to the operator and to environmental influences) and the *spatial variability* of the concrete performance properties due to differences of compaction and curing, possible non-uniform supply of material and structural effects (reinforcement, changes in dimension, corners, connecting structural elements etc.). Inherent variability phenomena can be considered as point properties (local parameter). Spatial variability phenomena can be considered as regional properties (regional or volume parameter). Local phenomena can be analysed by classical statistical methods. Analysis of regional phenomena needs spatial models – that are typically used in *geostatistics*.

Development of geostatistical tools is attributed to Prof. George *Matheron* who published his treatise on the Theory of Regionalised Variables and its Applications based on earlier empirical work in the 1960s [1], nevertheless, the basic idea of *kriging* (Gaussian piecewise-polynomial spline interpolation regression) is first used in a technical context by Prof. Danie G. *Krige,* in his study about average gold grades at the Witwatersrand reef complex in South Africa [2]. Historically, Prof. Andrey N. *Kolmogorov* was the first who recognized spatial correlation. He defined the so-called *structure function* for its representation and developed how to use the structure function for optimal interpolation (without bias and with minimum variance) [3]. *Kolmogorov* was unable to use the method due to the lack of computer power in those days [4]. *Kolmogorov*'s structure function is known today as the *variogram* and his interpolation technique as *kriging*.

Geostatistics deals with spatially autocorrelated data (autocorrelation = correlation between elements of a series and others from the same series separated from them by a given interval). Some spatially autocorrelated parameters of interest in geostatistics are facies, reservoir thickness, porosity, permeability [5].

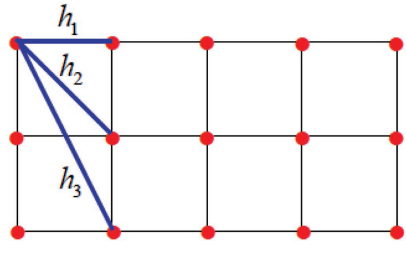

Fig. 1. Schematic representation of lag vectors in 2D [7]
1. ábra Kétdimenziós helyvektorok sematikus megjelenítése [7]

Geostatistics usually assumes that the differences between the values of samples are determined by the relative spatial orientation of the samples and the mean and variance of

the differences depend only on the relative orientation [6]. Therefore, the semivariogram is introduced in spatial correlation analyses that plots the semivariance of samples as the function of the separation between two spatial locations (referred to as *lag*).

For the development of the semivariogram, let us suppose a 2D field of values of a variable $f(x,y)$ as indicated in *Fig. 1*. Lags are schematically shown as h_1, h_2 and h_3.

For the determination of a semivariogram corresponding to a 2D field of values of a variable $f(x,y)$, the followings can be considered:

u vector of spatial coordinates (with 2D components *x* and *y*),
$f(\mathbf{u})$ variable under consideration as a function of spatial location,
h lag vector representing separation between two spatial locations,
$f(\mathbf{u}+\mathbf{h})$ lagged version of variable under consideration,
$N(\mathbf{h})$ the number of data pairs separated by lag **h**.

Semivariance $\gamma(\mathbf{h})$ can be determined for lag **h** as of Eq. (1):

$$\gamma(\mathbf{h}) = \frac{1}{2N(\mathbf{h})} \sum_{i=1}^{N(\mathbf{h})} \left[f(\mathbf{u}_i + \mathbf{h}) - f(\mathbf{u}_i) \right]^2 \quad (1)$$

Semivariance is a measure of the dissimilarity of the values. The empirical function of $\gamma(\mathbf{h})$ can be considered as a population parameter. The diagram showing the semivariance versus lag is referred to as the *semivariogram*.

Geostatistical analyses prefer using the semivariogram since the semivariogram tends to filter the influence of a spatially varying mean by averaging the squared differences of the variable. Also, the semivariogram can be applied whenever the covariance function cannot be defined. In such a case the semivariance may keep increasing with increasing lag, rather than leveling off, corresponding to an infinite global variance; and the covariance function is undefined [5].

2. Spatial variability analysis for in-situ rebound hammer testing

Typical relative strength variation for structural concrete in a wall is illustrated in *Fig. 2* [8]. The strength gradients are reasonably uniform due to gravity and the variations in compaction and supply is visible in the variability indicated by the relative strength contours. Anisotropy is always realised in the compressive strength of structural members in vertical direction (including columns, walls, beams and thick slabs).

Considering the bottom surface of a slab, the variability of the compressive strength in horizontal direction is expected to be random due to only compaction and supply inconsistencies. The study of the spatial variability of concrete performance properties is, therefore, reasonable to be carried out for a bottom surface of a slab where the vertical bias in the compressive strength is excluded and the clear random influences due to only compaction and supply differences can be analysed.

For such an analysis, the bottom surface of the top concrete slab of a framed, monolithic, subsoil concrete tunnel was selected, with dimensions of 25.0 m × 7.5 m with a thickness of 0.48 m. The studied region on the bottom surface was 22.0 m × 6.0 m.

A total number of 42 testing locations were selected for Schmidt rebound hammer testing. N-type original Schmidt rebound hammer was used. Eleven individual rebound index readings were recorded at each location. The measurements were performed by the same operator.

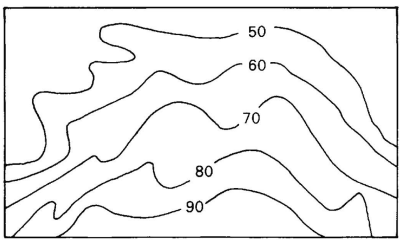

Fig. 2. Relative strength variation for a structural concrete wall [8]
2. ábra Relatív nyomószilárdság változása beton falban [8]

3. Results

The present paper discusses the spatial variability of the measured rebound indices (R_i) based exclusively on the statistical location parameters, i.e. test location *mean* – $E[R]$ values, test location *median* – $m[R]$ values and test location *mode* – $Mo[R]$ values.

A total number of 462 individual rebound indices were recorded at the 42 testing locations. The frequency histogram of the individual rebound indices without any separation by location is indicated in *Fig. 3* together with the best fit probability density function.

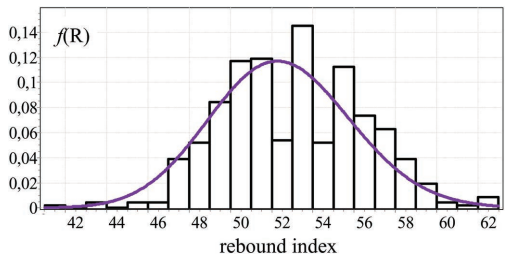

Fig. 3. Frequency histogram of the individual rebound indices for the 42 testing locations without any separation by location
3. ábra A 42 mérési helyen rögzített visszapattanási értékek együttes relatív gyakorisági hisztogramja

Considering the rebound hammer test, it can be assumed that the rebound index reading sets of separate testing locations are independent and identically distributed (i.i.d.) random variables since it can be supposed that the probability distribution of the rebound index does not change by location within the same concrete structure and the separate testing locations can be considered to be mutually independent [9]. Based on these assumptions, the central limit theorem applies for the rebound hammer test; i.e. the probability distribution of the mean of the rebound index reading sets of separate testing locations (each with finite mean and finite variance) approaches the normal distribution if sufficiently large number of the i.i.d. random variables is available. It can be realised that the mean of the 42 independent testing locations approaches rather well to the normal distribution.

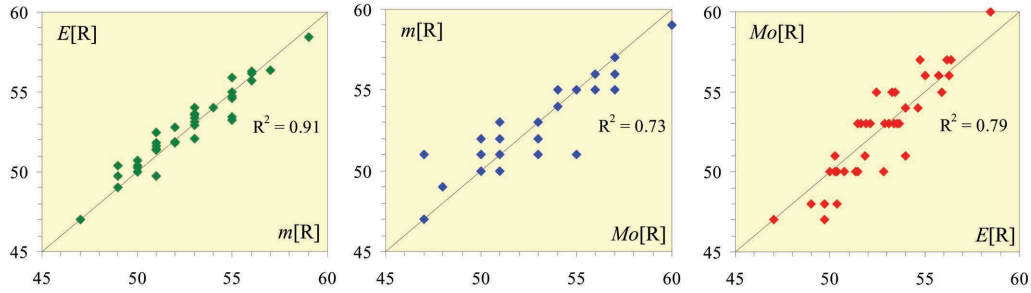

Fig. 4. Correlations between the mean, median and mode values for the 42 testing locations
4. ábra A visszapattanási értékek 42 mérési helyre vonatkozó átlagának, mediánjának és móduszának korrelációi

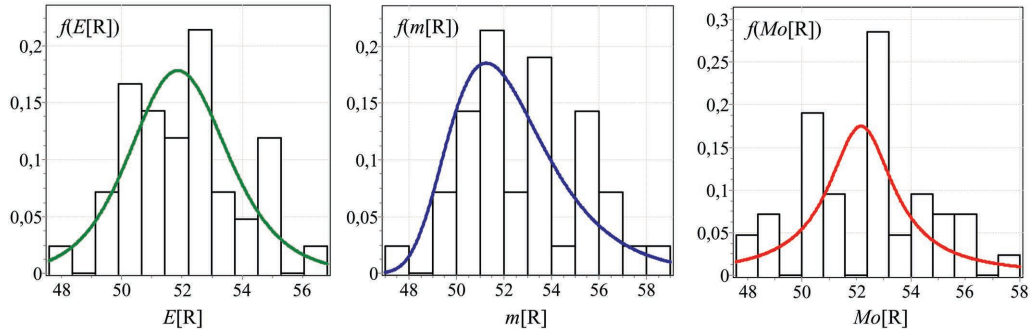

Fig. 5. Frequency histograms for the mean, median and mode values for the 42 testing locations
5. ábra A visszapattanási értékek 42 mérési helyre vonatkozó átlagának, mediánjának és móduszának gyakorisági hisztogramjai

For the 462 individual rebound indices, the global mean value is $E[R] = 52.6$, the global median value is $m[R] = 53$ and the global mode value is $Mo[R] = 53$. *Fig. 4* illustrates the rather close correlations between the statistical location parameters corresponding to the 42 testing locations.

Fig. 5 indicates the frequency histograms of the statistical location parameters; mean – $E[R]$ values, median – $m[R]$ values and mode – $Mo[R]$ values, respectively. Findings confirm that the three location parameters are not equally sensitive to the extreme individual values of which possible influences seem to rule out for the mean values (frequency histogram and best fit probability density function have almost zero skewness or excess kurtosis), on the contrary to the median values (where frequency histogram and best fit probability density function show positive skewness) and the mode values (where frequency histogram and best fit probability density function show positive excess kurtosis).

In a practical situation, when noticing or localising of the presence of eventually weaker regions of the structural element can be one purpose, the analysis of mean responses may be misleading; in the case of sufficiently large number of testing locations the central limit theorem applies and global observations can hide the influence of local extremities.

Contour plots may indicate local information in a visible way. Maps of the statistical location parameters for mean – $E[R]$ values, median – $m[R]$ values and mode – $Mo[R]$ values are shown in *Fig. 6,* respectively. It can be seen that the three parameters broadly show similar differences in the measured values, however, the extremities are observable the best at the contour plot of the mode values. Contour plot of the mean values seems to be the least sensitive in this sense. It can be also noted that different performance areas can be observed on particular maps that are not visible on the other two maps. Results evidently show the influences due to compaction and supply differences. The observed behaviour can be considered, however, result of random influences. No clear tendencies in the differences of the performance properties are realised.

In a practical situation, when eventually weaker regions of the structural element are present, it can be interesting to know that at which extent and in which orientation the discrepancy is present and has influence on performance properties. Geostatistical approaches can be used for the analysis of spatial variation. The method of kriging is applicable for modelling Gaussian random processes, based on models of semivariograms for a variable [1,4,6]. Semivariograms may indicate the lag distance (=*range*) over which the values of the variable are not correlated (independent). This distance can be referred to as *correlation distance*. The *sill* is the semivariance value at which the semivariogram levels off. The *nugget* is the semivariance value at distances smaller than the minimum lag of measurements [4,6]. Typical models for semivariograms are the spherical, exponential, Gaussian, wave, nugget [4-7]. Combined models are also used.

Fig. 7 represents the empirical semivariograms for the statistical location parameters; mean – $\gamma(E[R])$, median – $\gamma(m[R])$ and mode – $\gamma(Mo[R])$, respectively. The best fit spherical models are also indicated. It can be realised that the semivariogram models level off at a range about ten meters. In geostatistics, a common rule of thumb is accepted for the maximum lag in a semivariogram restricted to half of the diagonal of data extent [10]. In the present example, the concrete slab has dimensions of 25.0 m × 7.5 m of which the studied region is 22.0 m × 6.0 m. Semivariograms in *Fig. 7* are, however, not limited to about 12 meters since one dimension

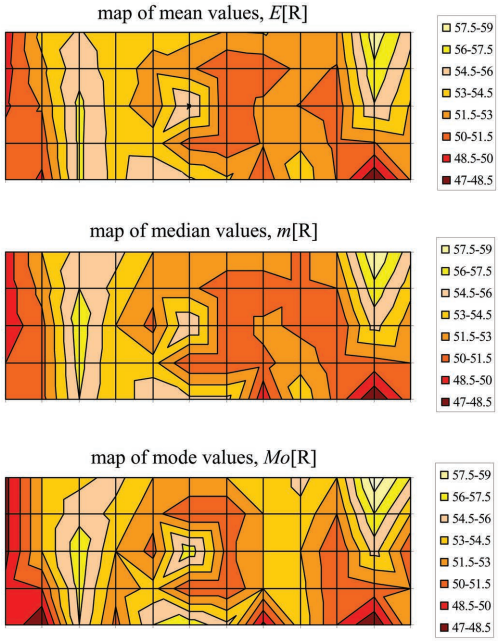

Fig. 6. Contour plots for the mean, median and mode values over the tested area
6. ábra A visszapattanási értékek átlagának, mediánjának és móduszának szintvonalas ábrázolása

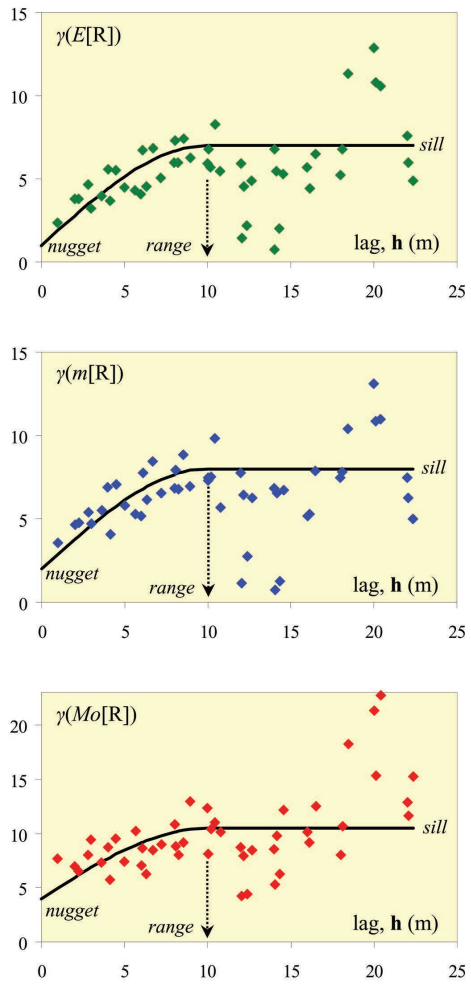

Fig. 7. Semivariograms for the mean, median and mode values for the 42 testing locations together with the best fit spherical model
7. ábra A visszapattanási értékek 42 mérési helyre vonatkozó átlagának, mediánjának és móduszának félvariogramjai, szférikus modellel közelítve

of the slab is three times larger than the other. Restricting the semivariograms at maximum lag about half of the diagonal of data extent would not allow the diagrams to visibly level off and the sill could not be clearly determined. It can be realised that the spatial variability of the mean and median values is of the same magnitude, and the spatial variability of the mode values is a little higher. It can be concluded that the testing locations can provide uncorrelated (independent) results for the rebound index readings over a lag distance of about ten meters.

4. Conclusions and future work

The present paper has summarised the application possibilities of particular geostatistical tools for modelling the spatial variability of rebound hammer non-destructive testing. Results of in-situ measurements were provided and analysed. The analysis of the inherent variability of the rebound hammer tests was limited to the comparison of the statistical location parameters; mean – E[R] values, median – m[R] values and mode – Mo[R] values. It was demonstrated that the statistical location parameters signify the inherent variability by different sensitivities. The spatial variability was analysed by contour plots and semivariograms of the statistical location parameters. It was demonstrated that the geostatistical methods may be applicable for the much smaller scale concrete structures than the scale of geological formations. Semivariograms and semivariogram models seem to be useful tools for the characterisation of spatial variability of concrete structures.

The spatial variability of geological and hydrological variables is well-described in the geostatistical literature for a long time. The use of the geostatistical methods for concrete structures is, however, still very much limited today. Further research is needed about the probability distribution of NDT measures and their influence on the boundary conditions for geostatistical methods. Size effect studies are also needed since the correlation distances are expected to be considerably different in particular cases – changing in the range of ten centimetres to ten meters –, depending on the actual workmanship and material supply. It is also of interest, which statistical parameter of the recorded NDT measure is the most suitable for a useful spatial variability analysis.

5. Acknowledgements

This research was supported by the Hungarian Scientific Research Fund project "Durability and performance characteristics of concretes with novel type supplementary materials" (OTKA K 109233) (Adorján Borosnyói) and by the European Union and the State of Hungary, co-financed by the European Social Fund in the framework of TÁMOP 4.2.4. A/1-11-1-2012-0001 'National Excellence Program' (Katalin Szilágyi).

References

[1] Matheron, G.: The Theory of Regionalised Variables and its Applications. Les Cahiers Du Centre De Morphologie Mathématique de Fontainebleau, No. 5, *École Nationale Supérieure des Mines de Paris*, 1 January 1971, 211 p.

[2] Krige, D. G.: A statistical approach to some basic mine valuation problems on the Witwatersrand. *Journal of the Chemical, Metallurgical and Mining Society of South Africa*, Vol. 52, No. 6, December 1951, pp. 119-139. http://dx.doi.org/10.2307/3006914

[3] Kolmogorov, A. N.: Interpolation and Extrapolation of Stationary Random Sequences (Интерполирование и экстраполирование стационарных случайных последовательностей). *Isvestia AN SSSR, Seriya Matematicheskaya (Известия АН СССР Серия математическая),* Vol. 5, No. 1, 1941, pp. 3-14. (in Russian) http://mi.mathnet.ru/izv3775
[4] Webster, R. – Oliver, M. A.: Geostatistics for Environmental Scientists. 2nd Ed., *John Wiley & Sons Ltd*, West Sussex, UK, 2007, 315 p. http://dx.doi.org/10.1002/9780470517277.ch1
[5] Bohling, G.: Introduction to Geostatistics and Variogram Analysis. Lecture notes for Data Analysis in Engineering and Natural Science, *Kansas Geological Survey, University of Kansas,* 17 October 2005, 20 p. http://people.ku.edu/~gbohling/cpe940/Variograms.pdf
[6] Clark, I.: Practical Geostatistics. *Geostokos Ltd,* Alloa, UK, 13 July 2001, 120 p. http://www.kriging.com/PG1979/PG1979.pdf
[7] Smith, T. E.: Notebook for Spatial Data Analysis. Lecture notes for Spatial Data Analysis with GIS Applications, *University of Pennsylvania, Department of Electrical and Systems Engineering,* 2 January 2013, 390 p. http://www.seas.upenn.edu/~ese502/#notebook
[8] Bungey, J. H. – Millard, J. H. – Grantham, M. G.: Testing of Concrete in Structures. *Taylor and Francis*, New York, 2006, 352 p.
[9] Szilágyi, K. – Borosnyói, A. – Zsigovics, I.: Extensive statistical analysis of the variability of concrete rebound hardness based on a large database of 60 years experience. *Construction and Building Materials,* Vol. 53, February 2014, pp. 333–347 http://dx.doi.org/10.1016/j.conbuildmat.2013.11.113
[10] Coombes, J.: Handy Hints For Variography. *Snowden Associates Ltd,* 2005, 16 p.

Ref.:
Adorján **Borosnyói** – Katalin **Szilágyi**: *Studies on the spatial variability of rebound hammer test results recorded at in-situ testing*
Építőanyag, 65. évf. 4. szám (2013), 102–106. p.
http://dx.doi.org/10.14382/epitoanyag-jsbcm.2013.19

Mérőhelyek közötti változékonyság értékelése Schmidt-kalapáccsal végzett helyszíni vizsgálat során
A helyszíni Schmidt kalapácsos vizsgálati eredmények változékonysága két hatásból tevődik össze: a mérőhelyi változékonyságból (ismételhetőség és reprodukálhatóság) és a mérőhelyek közötti változékonyságból, amely a térben eltérő bedolgozási és utókezelési hatások és az esetlegesen eltérő összetételű beton szállítmány eredménye. A mérőhelyi változékonyság statisztikai paraméterei a klasszikus matematikai statisztika eszközeivel kezelhetők. A mérőhelyek közötti változékonyság statisztikai paramétereinek vizsgálata térbeli statisztikai modelleket igényel, amelyeket a geostatisztika használ széles körben. A térbeli változékonyság leírására használt modelleket a geostatisztika szakirodalma részletesen, régóta tárgyalja. Ennek ellenére, vasbeton szerkezetek vizsgálatára e módszerek napjainkban még nem terjedtek el. A cikk bemutatja egy 25×7,5 m méretű vasbeton födém 22×6 m méretű szakaszának helyszíni schmidt kalapácsos vizsgálati eredményeit. A mérőhelyi változékonyság vizsgálata során bemutatjuk a mérési helyekre meghatározott helyzeti statisztikai jellemzők (számtani közép, medián, módusz) jellegzetességeik és egymáshoz viszonyított kapcsolatukat. Bemutatjuk, hogy a helyzeti statisztikai jellemzők más-más érzékenységgel jelzik a mérőhelyi változékonyságot. A mérőhelyek közötti változékonyság vizsgálata során bemutatjuk a helyzeti statisztikai jellemzők térbeli eloszlását és azok félvariogramjait. Bemutatjuk, hogy a geostatisztikában, nagy léptékben alkalmazott térbeli statisztikai modellek alkalmasak vasbeton szerkezetekre történő adaptálásra, kisebb léptékben is. A félvariogramok és azok közelítő modelljei alkalmasak a vasbeton szerkezetek helyszíni, Schmidt kalapácsos vizsgálati eredményeire vonatkozóan a mérőhelyek közötti változékonyság vizsgálatára.
Kulcsszavak: beton, felületi keménység, Schmidt kalapács, térbeli változékonyság, statisztikai helyzeti jellemzők, félvariogram

KÖNYVAJÁNLÓ ▪ BOOK REVIEW

Francis D. K. Ching
BUILDING STRUCTURES ILLUSTRATED

January 2014
ISBN: 978-1-118-45835-8
352 pages

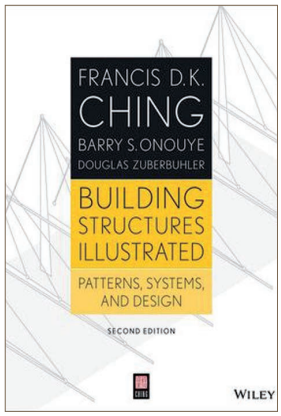

A new edition of Francis D.K. Ching's illustrated guide to structural design.
Structures are an essential element of the building process, yet one of the most difficult concepts for architects to grasp. While structural engineers do the detailed consulting work for a project, architects should have enough knowledge of structural theory and analysis to design a building. Building Structures Illustrated takes a new approach to structural design, showing how structural systems of a building—such as an integrated assembly of elements with pattern, proportions, and scale—are related to the fundamental aspects of architectural design. The book features a one-stop guide to structural design in practice, a thorough treatment of structural design as part of the entire building process, and an overview of the historical development of architectural materails and structure. Illustrated throughout with Ching's signature line drawings, this new Second Edition is an ideal guide to structures for designers, builders, and students.

- Updated to include new information on building code compliance, additional learning resources, and a new glossary of terms
- Offers thorough coverage of formal and spatial composition, program fit, coordination with other building systems, code compliance, and much more
- Beautifully illustrated by the renowned Francis D.K. Ching

Building Structures Illustrated, Second Edition is the ideal resource for students and professionals who want to make informed decisions on architectural design.

Costas Georgopoulos, Andrew Minson
SUSTAINABLE CONCRETE SOLUTIONS

February 2014, Wiley-Blackwell
ISBN: 978-1-119-96864-1
224 pages

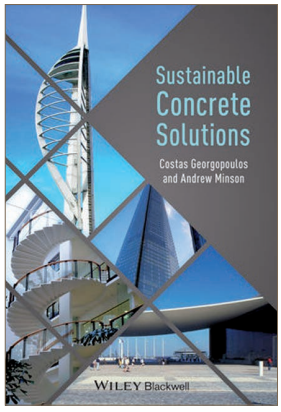

The challenges facing humanity in the 21st century include climate change, population growth, overconsumption of resources, overproduction of waste and increasing energy demands. For construction practitioners, responding to these challenges means creating a built environment that provides accommodation and infrastructure with better whole-life performance using lower volumes of primary materials, less non-renewable energy, wasting less and causing fewer disturbances to the natural environment. Concrete is ubiquitous in the built environment. It is therefore essential that it is used in the most sustainable way so practitioners must become aware of the range of sustainable concrete solutions available for construction. While sustainable development has been embedded into engineering curricula, it can be difficult for students and academics to be fully aware of the innovations in sustainable construction that are developed by the industry.

Sustainable Concrete Solutions serves as an introduction to and an overview of the latest developments in sustainable concrete construction. It provides useful guidance, with further references, to students, researchers, academics and practitioners of all construction disciplines who are faced with the challenge of designing, specifying and constructing with concrete.

Measurable properties of Al_2O_3 ceramic injection molding raw materials

ÁDÁM EGÉSZ ▪ GE Hungary Ltd., Budapest, Hungary ▪ adam.egesz@ge.com
LÁSZLÓ A. GÖMZE ▪ Department of Ceramics and Silicate Engineering, University of Miskolc, Miskolc, Hungary ▪ femgomze@uni-miskolc.hu

Received: 11. 12. 2013. ▪ Érkezett: 2013. 12. 11. ▪ http://dx.doi.org/10.14382/epitoanyag-jsbcm.2013.20

Abstract

Powder injection molding (PIM), which encompasses metal injection molding (MIM) and ceramic injection molding (CIM), is a process which enables large scale production of complex-shaped components for use in a diverse range of industries. Ceramic injection molding (CIM) is a technology for manufacturing complex, precision, netshape components from ceramic powder. In the illuminant industry, for producing arc tube parts for high intensity discharge lamps the applied method is the ceramic injection molding. The ceramic arc tube parts are made of high purity alumina powder. By producing ceramic parts, one of the most critical steps is to optimize the injection molding process, to determine and control the influential machine parameters, which have an effect on the quality of the end product. Nevertheless, the properties of injection molding raw material is needed to be known before any optimization of the injection molding process, because later the molding process is optimized for this material, to decrease the amount of cracked ceramics.

For producing ceramic arc tube parts (plugs), there are two different major components used for producing injection molding raw material (feedstock): high purity alumina powder as the main component, and an organic paraffin wax as a binder material. It is expressly important to know the physical and dimensional properties of the alumina powder, since mainly these have affect on the homogeneity and viscosity of feedstock, and therefore on the quality of the end product.

In the present research, both the main components and the moldable raw material were investigated by visual, physical, chemical and thermal methods. It was found – most importantly – that the viscosity of the raw material linearly decreases with the increasing grinding time of the alumina powder.

Applied analytical methods in terms of laser granulometry, tap density analysis, differential thermo-analysis and rheology analysis were used.

Keywords: alumina powder, paraffin wax, ceramic injection molding, laser granulometry, tap density, differential thermo-analysis, rheology analysis

Ádám Egész
Graduated in University of Miskolc, Department of Ceramics and Silicate Engineering as a material engineer, where he currently continues his studies as PhD student. He works at GE Lighting as project engineer, where he optimizes the manufacturing process of ceramic production for high intensity discharge lamps, especially the injection molding and its raw material. During his studies, he prepared several award-winning papers at Students' Scientific Workshops.

Prof. Dr. László A. Gömze
Establisher (in July 1st, 1999) and head of Department of Ceramics and Silicate Engineering in the University of Miskolc, Hungary. Since then 7 students from the department have successfully completed their PhD theses and 4 of them were managed by Prof. Gömze. Until today he is author of 2 patents, 4 books and more than 250 scientific papers. He was the chair of International Scientific Advisory Board of the international conferences ic-cmtp2 in 2012 and ic-rmm1 in 2013. Recently, he is the chair of the International Organization Board of the 3rd International Conference ic-cmtp3 on Competitive Materials and Technological Processes.

1. Introduction

Powder injection molding (PIM) is a technology for manufacturing complex, precision, netshape components from either metal or ceramic powder. The potential of PIM lies in its ability to combine the design flexibility of plastic injection molding and the nearly unlimited choice of material offered by powder metallurgy, making it possible to combine multiple parts into a single one. Furthermore, PIM overcomes the dimensional and productivity limits of isostatic pressing and slip casting, the defects and tolerance limitations of investment casting, the mechanical strength of die-cast parts, and the shape limitation of traditional powder compacts [1,2,10].

There are two different major components used for producing injection molding raw material (feedstock) in the illuminant industry for producing ceramic arc tube parts (plugs) for the High Intensity Discharge lamps: high purity alumina powder as the main component, and an organic paraffin wax as a binder material. The flow chart of injection molded ceramic parts production can be seen in *Fig. 1.*

Producing the feedstock, the wax is heated in a sigma-blade mixer, and the alumina powder is sequentially added to the molted wax material. The given, properly homogenized mixture is cooled down, and broke in jaw crusher to get granules from it. The granules can be used for the ceramic injection molding process (*Fig. 2*).

To know the physical, chemical and thermal properties of the given feedstock granules is absolutely necessary, if an efficient injection molding process is to be set up, which results a quality end product as well [3-6]. The most commonly occurring failures in the end product are the cracks, voids and different material discontinuities, and to avoid these failures, the best way is the qualification of raw materials.

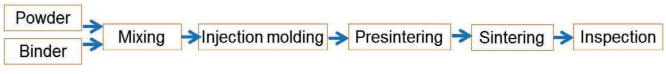

Fig. 1. Flow chart of injection molded ceramic production
1. ábra Kerámia fröccsöntés folyamatábrája

Fig. 2. Granules raw material, injection molded green- and end product (arc tube)
2. ábra Granulált alapanyag, félkész termék és késztermék (kisülőcső)

2. Experimental

To qualify the alumina powder and feedstock raw material, the following measuring methods were tested:

2.1. Laser granulometry

The laser granulometry method can be used to determine the grain size distribution of the usable powder, to qualify the alumina powder. Additionally to the grain size distribution, the grade of polydispersity (*Fig. 3*) and the compaction and volume filling properties of the powder can be determined and thus the density of the end product can be predestined [5,6,8,9,11,12,22-24]. The principle of the measurement is the following: the intensity-distribution of monochromatic parallel light beam is measured in the function of the scattering angle, when it has been transmitted through the sample. From this value, using different models and theories, the grain size distribution of the particles can be counted in the sample [7,10].

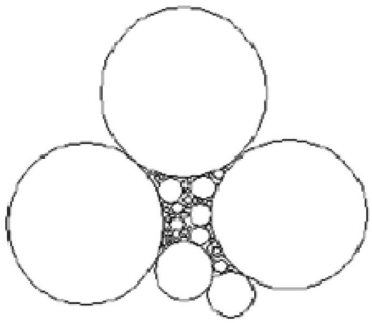

Fig. 3. Scheme of polydisperse alumina powder
3. ábra Polidiszperz alumínium-oxid por sémája

2.2. Tap dendity measurement

Tap density measurement can provide an alternative to the laser granulometry if do not have enough time and do not have opportunity to apply the relatively complicated and time-consuming laser granulometry method. In this way, the density and the grade of polydispersity of the powder can be determined [6,7,10]. The principle of the tap density measurement is the following: the given weight of alumina powder is put into a scaled cylinder that is laid on a resonator unit. The unit shakes the cylinder at defined vibration rate (*Fig. 4*). The volume of the vibrated powder is recorded after the vibration, and the tap density can be calculated by dividing the weight of the powder with its volume. The tap density, and so the appropriate grain size distribution of the powder can be adjusted with grinding in vibratory ball mill [13-18,25-27].

Fig. 4. Tap density measurement of alumina powder
4. ábra Alumínium-oxid por rázott sűrűség mérése

2.3. Differential thermo-analysis

The effect of heat during endothermic and exothermic reactions in solid materials can be measured using the well known differential thermo-analysis method. The investigated material is heated together with a comparative material (inert material). In the inert material no any endothermic or exothermic process or any phase transformation occurs in the temperature range used. By comparison, the phase transformations – and corresponding temperatures – are determinable in different materials, e.g. melting, evaporation or ignition temperatures [19,20,21].

In the studied case, the most important is to know the injection molding work temperature of the used raw material, since the process have to be adjusted to the proper temperature; which is above the melting temperature, but it is under the intensive evaporation temperature, to avoid the material loss during the injection molding process.

2.4. Rheological test

By injection molding it is necessary to know the rheological properties and the behaviour of raw materials, especially the viscosity. Mainly, this property defines the behaviour of the material during injection molding, and identifies the flow behaviour in the molding tool, thus it can have effect on the quality of the end product [28-35].

To define the viscosity of feedstock, dynamic rotational rheometer and capillary rheometer were used.

Besides of the raw material, to know the rheological properties of wax binder material can be also important, since mainly the binder material defines the rheological behaviour and viscosity of injection molding raw material [36,37,38].

3. Results and discussion

3.1. Laser granulometry

The first measurement to qualify the properties of the powder is the laser granulometry to investigate grain size distribution. The method is able to determinate the typical grain size and grain distribution of the alumina powder.

In the followings a comparison is given for a raw, unmilled and 10 minutes in vibration ball mill milled alumina powder. The grain distribution curve of unmilled powder can be seen in *Fig. 5*, where the two peaks on different grain sizes can be observed, which confirm the polydisperse grain size distribution mentioned earlier (*Fig. 3*).

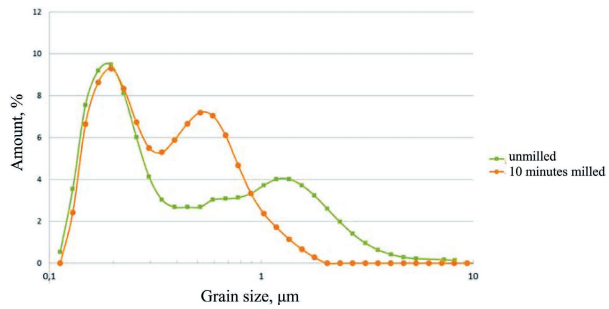

Fig. 5. Grain size distribution of unmilled and 10 minutes milled alumina powder
5. ábra Őröletlen és 10 percig őrölt alumínium-oxid por szemcseméret-eloszlása

The shape of the curve of the milled powder is clearly different (*Fig. 5*). It can be seen that the second peak is higher, but located closer to the first peak in the smallest grain size range, which indicates the presence of smaller particles and less pronounced polydisperse properties of the powder, but better compaction properties and higher density, due to the higher amount of small particles.

3.2. Tap density measurements

As it was mentioned earlier, the tap density and so the appropriate grain size distribution of the powder can be adjusted with grinding in vibratory ball mill.

In the experiment alumina powders with different initial grain size distributions were tested and grinded in vibratory ball mill. The initial average grain size was defined using laser granulometry. During the test the authors have applied different grinding times for the different powders. The tap density of the milled powders was determined after grinding.

The results of the experiment, the tap density of 4 powders with different initial grain sizes can be seen in *Fig. 6*. An exponential response can be found between the tap density and the grinding time since more small particles are produced during the grinding, which have better volume filling and compaction properties. The small particles can be wedged among the larger particles (polydisperse powder). It can be also realised that less grinding time is needed to get the same tap density if a powder with smaller initial grain size is used. It is in evidence that one can conclude from the measured tap density to the grain size of alumina powder.

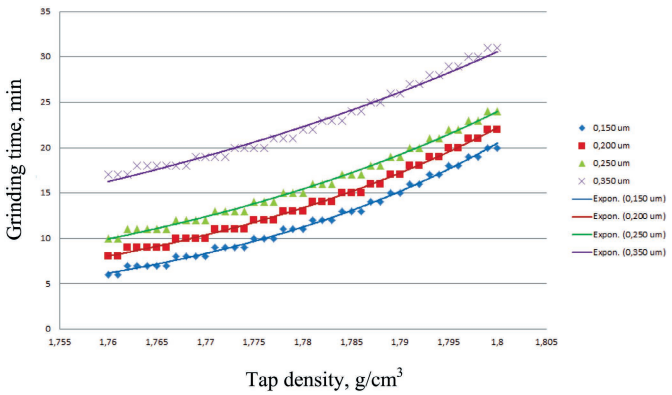

Fig. 6. Tap density of alumina powders vs. grinding time
6. ábra Alumínium-oxid porok rázott sűrűségének és őrlési idejének az összefüggése

3.3. Differential thermo-analysis

For the played out processes we can conclude from the weight changing of material. The feedstock material was experimentally tested by differential thermo-analysis and the graphical output can be seen in *Fig. 7*. The melting point (T_m) on the first negative peak, the evaporation point (T_e) on the first positive peak and the flashpoint (T_f) on the second positive peak of the material on the DTA curve can be observed.

3.4. Rheological test

The rheological properties of raw material were investigated by a dynamic rotational rheometer to define the flow properties of the material at different temperatures and shear velocities. This measurement is important since the flow properties of the material has influence on the injection molding process, and thus on the quality of the end product. The recorded viscosity curves for the feedstock material can be seen in *Fig. 8*.

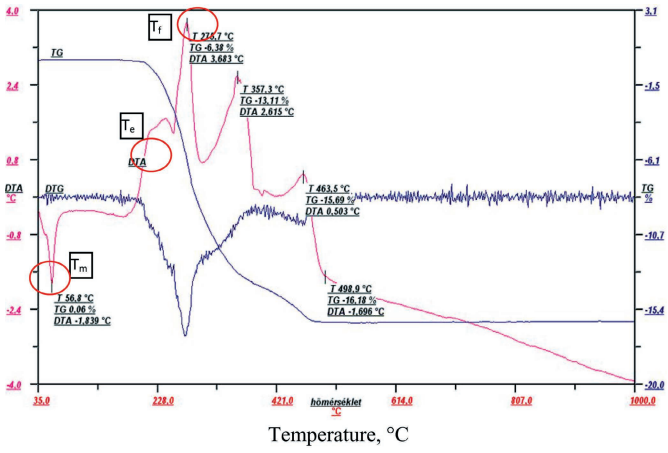

Fig. 7. Differential thermo-analysis of injection molding raw material
7. ábra Por fröccsöntési alapanyag derivatogramja

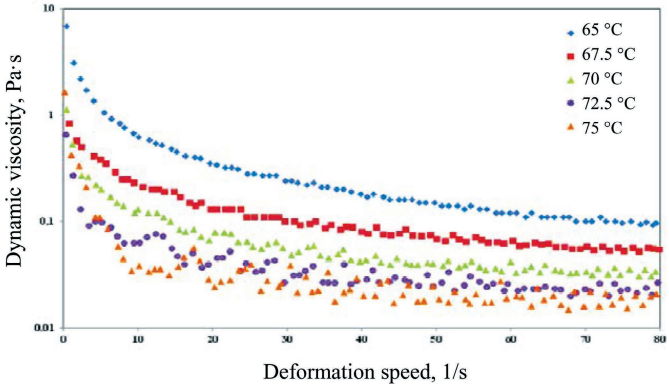

Fig. 8. Viscosity of injection molding raw material in the function of deformation speed and applied temperature
8. ábra Por fröccsöntési alapanyag viszkozitása a deformáció sebesség és a hőmérséklet függvényében

It can be realised that the viscosity decreases exponentially with the increasing deformation speed, and decreases with the increasing temperature.

The viscosity of the raw material was investigated in the function of initial tap density and milling time of alumina powder as well. Alumina powders with different initial tap densities were milled for different periods of time and then the raw material was mixed from them with adding wax binder. The viscosities of the different raw materials were measured at constant temperature of 68 °C by a capillary viscometer. The results of experiment can be seen in *Fig. 9*.

It can be concluded that the viscosity can be well adjusted with diversifying the milling time of the alumina powder, by given and constant mixing conditions, since the correlation is quasi linear between the milling time and viscosity, and the slope of the curves is quite similar. It can be observed that the viscosity of the different powder-made raw materials is decreasing with the increasing milling time. It is also visible that the powder with lower initial tap density needs to be

milled for a longer time to prepare a raw material with a given viscosity. The explanation for this phenomenon can be that the tap density is increasing with the milling time and there are more grains in a given volume with higher specific surface area where the binder material can adhere. It can decrease the internal friction of the raw material.

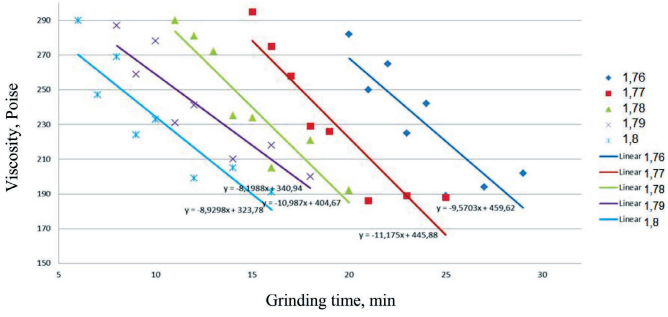

Fig. 9. Viscosity of injection molding raw materials with different initial tap density powder
9. ábra Por fröccsöntési alapanyagok viszkozitása eltérő rázott sűrűség esetén

4. Conclusions

It was demonstrated that the investigated measuring methods are suitable to qualify either the alumina powder, or the mixed injection molding raw material. The quality of the raw materials can be determined by the proposed investigations and the classification can be possible before use.

It is possible to determine the grade of polydispersity of the alumina powder by laser granulometry. The grade of polydispersity can be reduced in the alumina powder using vibration ball mill to enhance the volume filling performance.

The tap density measurement can be a good supplementary investigation for the grain size and grain size distribution of alumina powder.

The injection molding raw material can be characterized by differential thermo-analysis: evaporation, melting and ignition point can be found and the temperature work point for injection molding can be determined.

The dynamic viscosity of the injection molding raw material decreases exponentially with the increasing deformation speed, and decreases with the increasing temperature. It was observed that the rheological behaviour of the raw material depends more on the applied temperature than on the deformation speed gradient.

The dynamic viscosity of the different powder-made raw materials is decreasing with the increasing milling time. Alumina powder with lower initial tap density needs to be milled for a longer time to prepare a raw material with a given viscosity.

5. Acknowledgement

The paper was published with the permission of ic-rmm1, the 1st International Conference on Rheology and Modeling of Materials, 7-11 October 2013, Miskolc-Lillafüred, Hungary.

References

[1] Mutsuddy, B. C.: Ceramic Injection Molding, *Chapman and Hall*, 1995, 368 p.
[2] Hausnerova, B. – Marcanikova, L.: Rheological Characterization of Powder Injection Moulding using Feedstock Based on Aluminium Oxide and Multicomponent Water-Soluble Polymer Binder. *Proceedings* of Recent Advances in Fluid Mechanics and Heat & Mass Transfer, 2011, pp. 245-250.
[3] Krauss, V. A. – Pires, E. N. – Klein, A. N.: Rheological Properties of Alumina Injection Feedstocks. *Materials Research*, Vol. 8, No. 2, 2005, pp. 187-189. http://dx.doi.org/10.1590/S1516-14392005000200018
[4] Rak, Z. S.: New trends in powder injection moulding. *Powder Metallurgy and Metal Ceramics*, Vol. 38, No. 3-4, 1999 March–April, pp. 126-132. http://dx.doi.org/10.1007/BF02676037
[5] Stanimirovic, Z.: Injection Molded Mn-Zn Ferrite Ceramics. *Proceedings* of 27th International Conference on Microelectronics MIEL 2010, 2010, pp. 227-229. http://dx.doi.org/10.1109/MIEL.2010.5490493
[6] Wei, W. C. J. – Wu, R. Y. – Ho, S. J.: Effects of pressure parameters on alumina made by powder injection moulding. *Journal of the European Ceramic Society*, Vol. 20, No. 9, August 2000, pp. 1301–1310. http://dx.doi.org/10.1016/S0955-2219(99)00295-2
[7] Yin, H. Q. – Jia, C. C. – Qu, X. H.: Micro powder injection molding—large scale production technology for micro-sized components. *Science in China Series E: Technological Sciences*, Vol. 51, No. 2, 2008, pp. 121-126. http://dx.doi.org/10.1007/s11431-008-0023-y
[8] Kulkov, S. – Grigoriev, M.: Sintering of Al_2O_3 ceramics based on different sizes powders. *Építőanyag*, Vol. 62, No. 3, 2010, pp. 66-69. http://dx.doi.org/10.14382/epitoanyag-jsbcm.2010.13
[9] Csányi, T. J. – Gömze, L. A.: Impact of nitrogen atmosphere on sintering of alumina ceramics. *Építőanyag*, Vol. 60, No. 1, 2008, pp. 15-18. http://dx.doi.org/10.14382/epitoanyag-jsbcm.2008.4
[10] Gitzen, W. H.: Alumina as a ceramic material, *The American Ceramic Society*, Ohio, 1970, 264 p.
[11] Berecz, E.: Kémia műszakiaknak, *Nemzeti Tankönyvkiadó*, Budapest, 1991, 816 p.
[12] Bárczy, P.: Anyagszerkezettan, *Miskolci Egyetem*, 1998, 280 p.
[13] Messinig, G. L. – Mccauley, W. – Mazdiyasni, K. S. – Haber, R. A.: Advances in Ceramic, Ceramic Powder Science, *The American Ceramic Society*, 1987, Vol. 21
[14] Kok, M.: Production and mechanical properties of Al_2O_3 particle-reinforced aliminum alloy composites. *Journal of Materials Processing Technology*, Vol. 161, No. 3, 30 April 2005, pp. 381–387. http://dx.doi.org/10.1016/j.jmatprotec.2004.07.068
[15] Sevik, H. – Kurnaz, S. C.: Properties of alumina particulate reinforced aluminium alloy produced by pressure die casting. *Materials & Design*, Vol. 27, No. 8, 2006, pp. 676–683. http://dx.doi.org/10.1016/j.matdes.2005.01.006
[16] Filser, F. – Gauckler, L. J.: Keramische Werkstoffe, Kapitel 4: 4 Beispiele für strukturkeramische Werkstoffe, *ETH-Zürich*, Department of Materials, 2006
[17] Csányi, T. J.: Alumínium-oxid porkerámiák alakadási technológiai paramétereinek optimalizálása, különös tekintettel a mechanikai tulajdonságokra és a mikroszerkezetre, *PhD Thesis*, Miskolc, 2007
[18] Tisza, M.: Anyagvizsgálat, *Miskolci Egyetemi Kiadó*, 2001, 494 p.
[19] Sōmiya, S.: Handbook of Advanced Ceramics. Volume I: Materials Science. Amsterdam, *Elsevier*, 2003, 764 p.
[20] Tamás, F.: Szilikátipari laboratóriumi vizsgálatok, *Műszaki Könyvkiadó*, Budapest, 1970
[21] Enrique, J. E. – Ochandio, E. – Gazulla, M. F.: Chemical Analysis, in Engineered Materials Handbook, *ASM International*, Materials Park, OH, 1991. Vol. 4
[22] Funk, J. E. – Dinger, D. R.: Particle Packing, Part 2. Review of Particle Packing of Polydisperse Particle System, *Interceram*, 1992. 41 (3), 176-179.
[23] Stenger, F. – Mende, S.: Nanomilling in stirred media mills, *Chemical Engineering Science*, Vol. 60, No. 16, August 2005, pp. 4557–4565. http://dx.doi.org/10.1016/j.ces.2005.02.057
[24] Peukert, W.: Material properties in fine grinding, *International Journal of Mineral Processing*, Vol. 74, Supplement, 10 December 2004, pp. S3-S17. http://dx.doi.org/10.1016/j.minpro.2004.08.006

[25] Barth, H.: Modern Methods of Particle Size Analysis, *Wiley-Interscience*, New York, 1985, 320 p.
[26] Allen, T.: Particle Size Measurement, *Wiley-Interscience*, New York, 1981, 552 p.
[27] Serkowski, S. – Müller, M.: Vacuum granulation of ceramic powders – Device and ability, *Journal of Materials processing Technology*, Vol. 175, No. 1–3, 1 June 2006, pp. 382–386. http://dx.doi.org/10.1016/j.jmatprotec.2005.04.065
[28] Sathyjakumar, M. – Gnanam, F. D.: Influence of additives on density, microstructure and mechanical properties of alumina, *Journal of Materials Processing Technology*, Vol. 133, No. 3, 20 February 2003, pp. 282–286. http://dx.doi.org/10.1016/S0924-0136(02)00956-1
[29] Lowell, S. – Shields, J.: Powder Surface Area and Porosity, *Chapman and Hall*, New York, 1984, 250 p.
[30] Nivot, C. – Valdivieso, F. – Goeuriot, P.: Nitrogen pressure effects on non-isothermal alumina sintering, *Journal of the European Ceramic Society,* Vol, 26, No. 1–2, 2006, pp. 9–15. http://dx.doi.org/10.1016/j.jeurceramsoc.2004.10.006
[31] Cótica, L. F. – Paesano, A. Jr. – Zanatta, S. C. – de Medeiros, S. N. – da Cunha, J. B. M.: High-energy ball-milled (αFe_2O_3)(αAl_2O_3) system: A study on milling time effects, *Journal of Alloys and Compounds*, Vol. 413, No. 1–2, 9 March 2006, pp. 265–272. http://dx.doi.org/10.1016/j.jallcom.2005.05.046
[32] Mutsuddy, B. C.: Influence of Powder Characteristics on the Reology of Ceramic Injection Molding Mixtures, Fabrication Sci., 3, *Proceedings of the British Ceramic Society*, 1983. pp. 117-137.
[33] Mamata P. – Parag B.: Influence of Sucrose Addition on Rheology of Alumina Slurries Dispersed with a Polyacrylate Dispersant, *Journal of the American Ceramic Society*, Vol. 88, No. 4, April 2005, pp. 833-838. http://dx.doi.org/10.1111/j.1551-2916.2005.00183.x
[34] Bruni, G. – Lettieri, P. D.: An investigation of the effect of the interparticle forces ont he fluidization behaviour of fine powders linked with rheological studies, *Chemical Engineering Science*, Vol. 62, No. 1–2, January 2007, pp. 387–396. http://dx.doi.org/10.1016/j.ces.2006.08.059
[35] Edirisinghe, M. J. – Evans J. R. G.: Rheology of Ceramic Injection Molding Formulations, *British Ceramic Transactions*, Vol. 86, No. 1, 1987, pp. 18-22.
[36] Tanaka, T. – Saitoh, K. – Satoh, M. – Miyazaki, M. – Kaneko, Y.: Injection Molding of Alumina, *Yogyo-Kyokai-shi, Journal of the Ceramic Association, Japan* Vol. 93 (1985) No. 1081, pp. 572-576. http://dx.doi.org/10.2109/jcersj1950.93.1081_572
[37] Cima, M. J. – Lewis, J. A.: Binder Distribution in Ceramic Greenware during Thermolysis, *Journal of the American Ceramic Society*, Vol. 72, No. 7, July 1989, pp. 1192–1199. http://dx.doi.org/10.1111/j.1151-2916.1989.tb09707.x
[38] Csányi, J.: Rheological characteristics of alumina powders in dry pressing technology. *Építőanyag*, Vol. 61, No. 1, 2009, pp. 6-10. http://dx.doi.org/10.14382/epitoanyag-jsbcm.2009.2

Ref.:
Ádám **Egész** – László A. **Gömze**: *Measurable properties of Al_2O_3 ceramic injection molding raw materials*
Építőanyag, 65. évf. 4. szám (2013), 107–111. p.
http://dx.doi.org/10.14382/epitoanyag-jsbcm.2013.20

Al_2O_3 kerámia fröccsöntés alapanyagának vizsgálatai

A por fröccsöntés – amely magában foglalja a fém fröccsöntést és a kerámia fröccsöntést is – olyan folyamat, amely lehetővé teszi bonyolult, összetett geometriájú termékek alakadását nagy darabszámban az ipar számos ágazata számára. Kerámia fröccsöntéssel komplex, precíziós termékek állíthatók elő kerámiapor felhasználásával. A fényforrásiparban a kisülőlámpák kerámia alkatrészeinek alakadása fröccsöntéssel történik. A kerámia kisülőcső-alkatrészek alapanyaga nagytisztaságú alumínium-oxid por. Az alkatrészek előállításánál a legkritikusabb folyamatlépés a fröccsöntés, ezért optimalizálni, szabályozni szükséges azon paramétereit, melyek hatással lehetnek a végtermék minőségére. Ehhez meg kell ismernünk a felhasználandó fröccsöntési alapanyag tulajdonságait, kritikus paramétereit, hogy ezeket szabályozva egy robosztusabb fröccsöntési folyamatot állíthassunk be. A kerámia alkatrészek gyártásához a fröccsöntési alapanyagnak két fő alkotója van: nagytisztaságú alumínium-oxid por és paraffin viasz kötőanyag. Különösen fontos, hogy ismerjük az alumínium-oxid por fizikai, kémiai és morfológiai tulajdonságait, mert főként ezek vannak hatással az elkészített fröccsöntési alapanyag homogenitására, viszkozitására, és így a végtermék minőségére. Jelen tanulmányban a fröccsöntési alapanyag, valamint annak mindkét alkotóeleme tulajdonságait vizsgáltuk vizuális, fizikai, kémiai és termikus elemzési módszerekkel. A vizsgálatok alapján legfontosabb megállapításként elmondható, hogy a fröccsöntési alapanyag viszkozitása lineárisan csökken az alumínium-oxid por őrlési idejének növelésével. Az alkalmazott vizsgálati módszerek a lézer granulometria, a rázott sűrűségmérés, a differenciál termoanalízis és a reológiai analízis voltak.
Kulcsszavak: alumínium-oxid por, paraffin wax, kerámia fröccsöntés, lézer granulometria, reológia, rázott sűrűség

Experiments on the buckling behaviour of glass columns. Part 2.

Kinga NEHME ▪ Assoc. Prof., University of Debrecen, Department of Civil Engineering ▪ kpankhardt@yahoo.com
András JAKAB ▪ civil engineer, Üveg-Fémszer Kft. ▪ jakabandreas@gmail.com
Salem Georges NEHME ▪ Assoc. Prof., BME, Department of Construction Materials and Engineering Geology ▪ sgnehme@yahoo.com

Érkezett: 2013. 10. 16. ▪ Received: 16. 10. 2013. ▪ http://dx.doi.org/10.14382/epitoanyag-jsbcm.2013.21

Abstract
The authors demonstrated in a separate paper [1] the buckling behaviour of load-bearing glass columns and also the load bearing capacity issues of glass fins based on laboratory experiments. Present paper focuses on load-bearing glass columns and the stability issues of glass fins based on existing calculation methods of the critical load of glass columns. Authors compare the results of the laboratory experiments and theoretical calculations. The results are analysed with the calculation procedures in the focus of the international literature. The laboratory experiments were carried out at the BME, Department of Construction Materials and Engineering Geology. More than 60 specimens where loaded until fracture. Based on the experimental and theoretical results, the critical load was determined and the fracture and stability processes were illustrated by force-deflection diagrams. The critical load vs. slenderness responses were determined for fins consisted of monolithic (single layer glass) and laminated glass as well.
Keywords: glass column, buckling, load bearing glass, stability, transparency

Kinga NEHME
MSc Civil Engineer, PhD, Associate Professor at the Department of Civil Engineering, University of Debrecen. Owner of Struktúra Ltd. engineering office (design, quality control). Member of the Technical committee of Glass Working Group (MSZT/MB 112) of Hungarian Standardization Institute; Hungarian Group of fib; Hungarian engineer chamber (MMK: 01-9160). Fields of interests: load bearing glasses, testing of construction materials, design, recycling of building materials.

András JAKAB
MSc Civil Engineer, designer at Üveg-FémSzer Ltd. Fields of interests: glass construction, glass columns, construction technology and management.

Salem G. NEHME
MSc Civil Engineer, PhD, Associate Professor at the Department of Construction Materials and Engineering Geology, Budapest University of Technology and Economics (BME). Member of the Technical committee of Glass Working Group (MSZT/MB 112) of Hungarian Standardization Institute; Hungarian Group of fib; Hungarian engineer chamber (MMK: 01-9159). Fields of interests: concrete technology, mass concrete, self-compacting concrete, fibre reinforced concrete, quality control of building materials, non-destructive testing, reinforced concrete structures, recycling of concrete.

1. Introduction

Heat-treatment procedure is the most often used glass strengthening method for building glasses. Two different types of so-called pre-stressed glass are produced with the heat strengthening method: tempered and heat strengthened glass. With lamination of several glass panes, multi-layered (hereinafter laminated) glass is produced. The interlayer material serves two purposes: *(i)* to keep glass splinters in place during the fracture process to reduce the risk of injury and *(ii)* to increase residual load bearing capacity [2, 3]. Interlayer material used in laminated glass is EVA (ethyl-vinyl-acetate) foil.

The structural behaviour of laminated glass lies between two limits, the so-called *lower (layered) limit*, where the glass panes react without a shear bond and the *upper (monolithic) limit*, where all glass panes are rigidly connected. For both limits, stresses in the glass panes can be calculated using the known formulas and models. In reality, the maximum stress of the laminate lies between those two limits. Calculation methods and formulae for the buckling force should match these ultimate values.

The most known formula is *Euler*'s formula to determine the critical load (hereinafter critical force) of a column. Question arises: Can be this formula applied for glass columns consisted of single layer glass and for laminated glass as well?

In the international literature four formulae for the buckling force of laminated glass columns exist. One of the formulae results in conservative values of the critical buckling force [4], one of them results correct values in the "lower" and "upper" limits of the critical buckling force [5], and one of them results in correct "lower" and conservative "upper" limit of the critical buckling force [6]. Three of the formulae [4,5,6] do not contain a distinct parameter which controls the transition from the lower to the upper limit of the critical buckling force. One of the formulae [7] introduces a coupling parameter which controls the transition between the lower and the upper limit of buckling force of laminated glass columns.

Further question arises: Can be all these formulae applied for glass columns consisted of float glasses and for heat-strengthened glass as well?

2. Experimental and theoretical studies

2.1 Influencing factors of buckling behaviour of glass columns

To perform engineering calculations, the affecting factors on glass and interlayer material (e.g. effect of tempering should be studied) should be supplemented by laboratory testing.

Different influencing factors should be taken into account for the calculation of buckling behaviour and strength of a single or laminated glass pane. According to *Wölfel*'s calculations [8], the primary interlayer property that influences the strength and deflection is the shear modulus, *G*, of the interlayer. In the case of thin or large size glass, where the deformations (deflections) are considerable, temperature dependent flexural stiffness (D_{fl}) of the overall laminate is more significant.

The following main influencing factors on the buckling behaviour of glass columns were experimentally studied:

- effect of thickness of glass pane,
- effect of number of glass layers,
- effect of heat-strengthening,
- effect of slenderness of critical force of glass column.

2.2 Laboratory experiments

2.2.1 Test parameters

Laboratory experiments were carried out to study the buckling behaviour of single and laminated glass columns at

the Department of Construction Materials and Engineering Geology, BME. All glass specimens were loaded in compression by concentrated load by variable specimen heights and a constant nominal width of 80 mm.

Single layer float glass, single layer heat-strengthened glass and laminated glass consisted of both float and heat-strengthened glass layers were tested. Although single layer glass and float glass are usually not used in load bearing glass columns, the effect of heat-strengthening on the buckling behaviour can be studied and can be compared with existing calculation methods in this way. The experimental procedure and test set-up is presented in [1].

Test parameters of glass specimens were the followings [1]:

Constants: test arrangement, the type of support; width of glass (80 mm); interlayer material (EVA foil with thickness of 0.38 mm); edgework; temperature (+23 ± 5 °C).

Variables: type of glass layers: HSG/ non heat-treated Float; height of specimens: 1000 mm; 920 mm; 840 mm; number of glass layers and the thickness of specimens: single layer: 8 mm; 12 mm, laminated: 2×4 mm; 2×6 mm; 8+4 mm, laminated: 3×4 mm; The rate of loading: 0,5 mm/min; 1 mm/min.

Support: Height of fixing: 95 mm; rubber plate (Shore A 80) was used between the steel supports and the glass.

Simplified designation is used to distinguish the studied specimens; e.g. *H_2(4.4)_2_920_0.5*

- H, F: Type of glass: H – HSG; F – non heat-treated float glass;
- 2(4.4): Number of glass layers e.g.: 2×4 mm laminated glass;
- 2: The number of specimen;
- 920: Nominate height of specimen [mm];
- 0.5: Rate of loading [mm/min].

3. Calculation methods for buckling of glass columns

3.1 Critical force of glass columns consisted of single layer glass

3.1.1 Calculation of critical force with Euler's method

The buckling behaviour of the single layer (monolithic) glass and that of laminated glass with rigidly bonded glass layers (upper limit) is similar to the buckling behaviour of an ideal elastic rod tested in compression. In this case the calculation of the critical buckling force can be determined with *Euler*'s method. *Euler*'s formula is the basis of the calculations for the critical buckling force of glass columns.

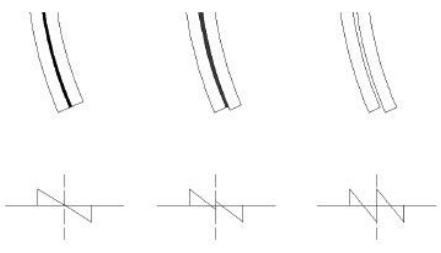

Fig. 1. a) monolithic behaviour, b) real behaviour; c) lower (layered) limit
1. ábra a) Monolitikusan együttdolgozó, b) Valós viselkedés c) Nem együttdolgozó rétegek

The critical buckling force of glass columns with *Euler*'s formula can determined as follows (*Eq. 1*):

$$N_{cr} = \frac{\pi^2 \cdot E \cdot I}{L_{cr}^2} \quad (1)$$

where:

N_{cr} – critical force;
L_{cr} – critical buckling length;
E – Young's modulus of glass;
I – moment of inertia.

3.2 Calculation of critical force of glass columns consisted of laminated glass

Authors have compared the results of the laboratory experiments and theoretical calculations. The results were analysed with the calculation procedures in the focus of the international literature. Simplified designation is used for the studied calculation methods of critical buckling force of laminated glass tested in compression, where in the designations in the lower indices mean:

L – Single glass layers (without use of foil interlayer material);
O – Laminated glass, with non-bonded glass layers („lower limit", with use of foil interlayer material);
U – Laminated glass, with rigidly bonded glass layers („upper limit", with use of foil interlayer material);
F – Foil interlayer material in laminated glass.

3.2.1 *Allen's* method

The calculation method of *Allen* [4] should be used only in the case of laminated glass with use of symmetrical glass layer thicknesses (laminated glass consisted of glass layers and interlayer material with similar thicknesses). In this formula the shear modulus of the interlayer foil material influences the critical buckling force of the glass column. The formula results in conservative values of the critical buckling force (*Eq. 2*).

$$N_{cr} = \frac{N_{cr,O}}{1 + \frac{2 \cdot N_{cr,O}}{\left[\frac{G_f \cdot b \cdot \left(v_f + v\right)^2}{v_f}\right]}} \quad (2)$$

where:

$N_{cr,O}$ – critical buckling force of laminated glass "lower limit";
G_f – shear modulus of the foil interlayer material;
v_f – thickness of the foil interlayer material;
v – thickness of the glass layer;
b – width of the glass column.

3.2.2 Method of *Sattler* et al.

The formula by *Sattler* et al. (see *Eq. 3*) results correct values in the "lower" and "upper" limits of the critical buckling force and can be applied in the case of with non-symmetrical layered laminated glass as well.

$$N_{cr} = \frac{\pi^2 \cdot \left(1 + \alpha + \pi^2 \cdot \alpha \cdot \beta\right)}{1 + \pi^2 \cdot \beta} \cdot \frac{D_O}{L_{cr}^2} \quad (3)$$

where:

D_O – bending stiffness of laminated glass "lower limit";
α – coefficient depending on the moment of inertia;
β – coefficient depending on the stiffness;
L_{cr} – the critical buckling length.

3.2.3 *Zenkert's* method

The formula by *Zenkert* (see *Eq. 4*) results in correct "lower" and conservative "upper" limit of the critical buckling force and can be applied in the case of with non-symmetrical layered laminated glass as well.

$$N_{cr} = \frac{\frac{\pi^4 \cdot D_L \cdot D_O}{D_f \cdot L_{cr}^4} + \frac{\pi^2 \cdot D_O}{L_{cr}^2}}{1 + \frac{\pi^2 \cdot D_O}{D_f \cdot L_{cr}^2}} \quad (4)$$

where:

D_L – bending stiffness of single glass layers in laminated glass;
D_O – bending stiffness of non-bonded glass layers;
D_f – bending stiffness of foil;
L_{cr} – the critical buckling length.

3.2.4 *Blaauwendraad's* method

The dimensionless ξ parameter in (see *Eq. 5*) controls the contribution of the foil between the two glass layers.

$$N_{cr} = (1-\xi)\cdot N_{cr.L} + \xi \cdot N_{cr.U} \quad (5)$$

where:

N_{cr} – critical buckling force (in the indices *L*: the "lower limit", *U*: the "upper limit");
x – coupling parameter ;
f – flexibility of the layers (in the indices *1, 2:* glass layer No. 1 and No. 2 , *f*: foil interlayer material).

The coupling parameter (see *Eq. 6*) should be determined in the case of laminated glass consisted of two glass layers:

$$\xi = \frac{f_1 + f_2}{f_1 + f_f + f_2} \quad (6)$$

The modified coupling parameter *(3.7)* is in the case of laminated glass consisted of three glass layers:

$$\xi = \frac{f_1 + f_2 + f_3}{f_1 + f_f + f_2 + f_f + f_3} \quad (7)$$

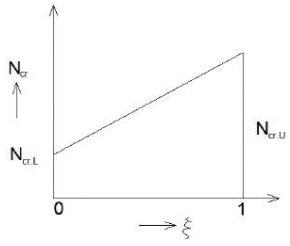

Fig. 2. Coupling parameter (ξ)
2. ábra Kapcsolati tényező (ξ)

Fig. 2. indicates the possible range of the values of the coupling parameter, $\xi = 0$ in the case of laminated glass consisted of non-bonded glass layers and $\xi = 1$ in the case of monolithically bonded glass layers.

4. Experimental and theoretical results

4.1 Influencing factors of buckling behaviour of glass columns

4.1.1 Effect of support type

The supporting structures of glass columns are usually designed as fixed connections e.g. steel shoe [1], where damping material e.g. hard rubbers or plastics is placed between the surfaces of the glass and the steel plate, to avoid high stress concentrations in the contacting area. Due to different load histories (e.g. wind load) of a façade glazing, the glass fin deforms as well. During the load transfer of a glass fin to the supporting structure, deformations occur in the damping material, therefore the effect of the initial geometrical imperfections increase. In this paper the authors focus on structural elements without geometrical imperfections (study of geometrical imperfections is aim of future work). In the case of high compression of the damping material, or use of soft rubbers, as well as inappropriate finishing (e.g. rotation of the fin within the support) the initially designed fixed support behaves rather as a pinned connection. *Fig. 3.* indicates the importance of the type of the support, which influences the critical buckling force. The critical buckling force increases in the supporting structure in the case of reduced rotations of the glass fin.

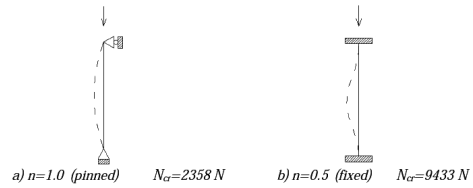

a) n=1.0 (pinned) Ncr=2358 N b) n=0.5 (fixed) Ncr=9433 N

Fig. 3. Critical buckling force and schematic buckling shape of a float glass specimen with 1000 mm height and 8 mm thickness, in the case of a) pinned and b) fixed support
3. ábra 1000 mm magas 8mm vastag float üveg próbatest kritikus ereje és sematikus kihajlási alakja, a) csuklós és b) befogott kapcsolat esetén

The deformations of the specimens were recorded with Olympus high speed camera. The deformed shapes of the specimens during the buckling behaviour were studied. Three different stages can be distinguished in the buckling behaviour of glass columns. In the 1st Stage the elastic deformation of the damping material (rubber plates) influences the vertical and horizontal displacements and no buckling occur (first stable stage). The 2nd Stage is a short term stage which indicates a geometrical instable condition (in which direction the buckling will occur) and the specimen loses its former stability (bound phenomenon, instability). The 1st and 2nd Stages are mainly influenced by the initial supporting conditions (e.g. quality of finishing work) and type of the fixing varies until the ultimate deformation of the damping material under loading conditions. Before the 3rd Stage, visible inflexion points in the buckling shape can be distinguished, see *Fig. 4.*

The most dense fragmentation pattern can be observed in the fractured specimens in the region of the inflexion points. In the 3rd Stage both the vertical and the horizontal displacements increase until fracture of glass (second stable stage). This Stage is less influenced by the initial supporting conditions. The continuous compression of the elastic damping material during loading leads to variable supporting conditions, therefore the coefficient of fixing *(n)* changes during the test.

The coefficient of fixing *(n)* should be determined to compare the results of laboratory experiments and those of the calculation methods. The coefficient of fixing *(n)* was determined with use of the test results of single layer float glass. Coefficient of

fixing *n=0.645* was applied in the analytical study of different calculation methods of the critical buckling force (N_{cr}).

Table 1. summarises the main physical properties of glass and interlayer material used in the calculations.

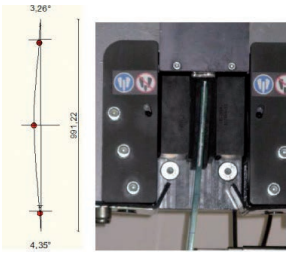

Fig. 4. Buckling shape in the region of the upper support (3rd Stage)
4. ábra Kihajlási alak a felső megtámasztás környezetében (3. szakasz)

Properties	Unit	Glass	EVA foil
Specific gravity	g/cm³	2.5	0.95
Thickness	mm	variable	0.38
Young's modulus at 23±2 °C	N/mm²	70000	1.2 <
Shear modulus at 23±2 °C	N/mm²	29200	4.54
Poisson ratio at 23±2 °C	-	0.23	0.32

Table 1. Main physical properties of glass and EVA foil interlayer material [2]
1. táblázat Üveg és EVA fólia laminálló anyag főbb fizikai jellemzői [2]

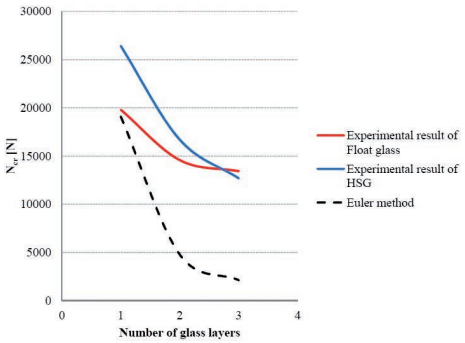

Fig. 5. Critical buckling force with Euler's formula in the case of single and laminated glass of 1000 height, consisted of float or HSG glass and that of tested glass vs. number of glass layers
5. ábra Euler-féle elmélettel számított 1000 mm magas, float vagy HSG üvegből felépülő egy és többrétegű (nem együttdolgozó) üvegek valamint a kísérleti üvegek kritikus teher értékei, az üveg rétegszámának függvényében

4.1.2 Calculation of critical force with *Euler's* formula

The calculation method of the critical buckling force with *Euler*'s formula does not distinguish between float and heat-strengthened (HSG) glass. *Fig. 5.* indicates the experimental results of single layer and laminated glass consisted of float or HSG glass layers with total thicknesses of 12 mm and also indicates the calculated values with *Euler*'s formula. Based on the experimental and theoretical results, *Euler*'s formula should be applied only in the case of float, monolithic single layer glass to determine the critical buckling force.

4.1.3 Critical buckling force based on the experiments and theoretical formulae

Table 2. summarises the calculated and experimental results of the critical buckling force. Although *Euler*'s formula should be applied only in the case of single layer float glass, the authors suggest the values also for further types of tested glass specimens for observation purposes.

The critical buckling force with *Sattler*'s formula overestimates the experimental values in the case of laminated glass consisted of float glass and gives correct values in the case of laminated glass consisted of HSG glass. The critical buckling force with *Allen*'s and *Zenkert*'s formulae result the same, usually lower, conservative values compared to the experimental results. The critical buckling force with the use of the *Blaauwendraad*'s formula results the most conservative lowest values. In the case of the *Blaauwendraad*'s formula both the "lower limit" and the"upper limit" can be determined (*Fig. 6*). *Table 3.* indicates the quantitative comparison of calculated and experimental results of the critical buckling force.

4.1.4 Effect of heat-strengthening

Euler's formula should not be applied in the case of HSG or laminated glass. All of the studied theoretical formulae result conservative values in the case of laminated glass consisted of HSG glass layers. The heat-strengthening increases the critical buckling force of glass columns. In the case of a single layer HSG glass with height of 1000 mm the critical buckling force increased with ~30 % compared to that of float glass.

4.1.5 Effect of number of glass layers

Based on the experimental results, the buckling force decreases with the increase of the number of glass layers in laminated glass. In *Fig. 5.* the number of the applied glass layers in laminated glass is indicated. The influence of the stiffness (and the effect of the shear modulus) of the interlayer material is increased in the case of laminated glass by the increase of the number of glass layers.

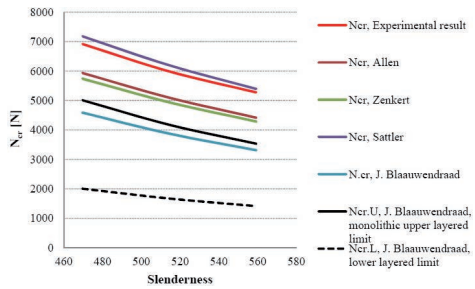

Fig. 6. Critical buckling force vs. slenderness of laminated glasses consisted of HSG 4.4 glass layers based on theoretical calculations and laboratory experimental results
6. ábra Laminált HSG 4.4 üvegek kritikus teher és karcsúság összefüggése, különböző számítási eljárások és a laboratóriumi kísérleti eredmények alapján

4.1.6 Effect of slenderness on critical force of glass column

Based on the theoretical calculations and laboratory experimental results, *Fig. 6.* indicates the critical buckling force vs. slenderness of laminated glass consisted of two HSG glass layers with thickness of 2×4 mm. In the case of *Blaauwendraad*'s formula both the "lower limit" and the "upper limit" were determined. *Blaauwendraad*'s formula results correct values in the case of laminated glass consisted of float glass layers, but in the case of HSG glass a shift factor of the coupling parameter, ξ should be introduced. In the case of conservative engineering calculations the use of *Blaauwendraad*'s formula is suggested.

Height *[mm]*	Type of glass	Number of glass layers *[mm]*	Critical buckling force (N_{cr}) *[N]*					
			Experimental results	Euler	Allen [4]	Zenkert [5]	Sattler [6]	Blaauwendraad [7]
1000	Float	1(8)	5672	5657	-	-	-	-
		1(12)	19803	19091	-	-	-	-
		2(4.4)	3490	1414	4428	4299	5409	3319
		2(6.6)	14575	4773	12028	12224	16869	11562
		3(4.4.4)	13425	2121	13361	13844	15208	9471
	HSG	1(8)	7506	5657	-	-	-	-
		1(12)	26420	19091	-	-	-	-
		2(4.4)	5278	1414	4417	4289	5397	3315
		2(6.6)	16699	4773	13259	12835	16206	10524
		2(8.4)	17495	6364	12028	12224	16869	11562
		3(4.4.4)	12684	2121	13361	13844	15208	9471
920		1(8)	8784	6683	-	-	-	-
		2(4.4)	5989	1671	5097	4939	6197	3875
840		1(8)	10207	8017	-	-	-	-
		2(4.4)	6919	2004	5935	5741	7179	4587

Table 2. Results of experiments and calculation methods
2. táblázat A kísérletileg mért értékek és a számítási módszerek eredményei

Height *[mm]*	Type of glass	Number of glass layers *[mm]*	Ncr *[N]*	Ratio of critical force of calculated and experimental values *[%]*				
			Experimental results	Euler	Allen [4]	Zenkert [5]	Sattler [6]	Blaauwendraad [7]
1000	Float	1(8)	5672	100	-	-	-	-
		1(12)	19803	96	-	-	-	-
		2(4.4)	3490	41	127	123	155	95
		2(6.6)	14575	33	83	84	116	79
		3(4.4.4)	13425	16	100	103	113	71
	HSG	1(8)	7506	75	-	-	-	-
		1(12)	26420	72	-	-	-	-
		2(4.4)	5278	27	84	81	102	63
		2(6.6)	16699	29	79	77	97	63
		2(8.4)	17495	36	69	70	96	66
		3(4.4.4)	12684	17	105	109	120	75
920		1(8)	8784	76	-	-	-	-
		2(4.4)	5989	28	85	82	103	65
840		1(8)	10207	79	-	-	-	-
		2(4.4)	6919	29	86	83	104	66

Table 3. Quantitative comparison of results of experiments and calculation methods
3. táblázat A kísérletileg mért értékek és a számítási módszerek eredményeinek kvantitatív összehasonlítása

5. Conclusions

a) The following conclusions can be drawn based on the theoretical calculations:

- The critical buckling force increases in the case of reduced rotations of the glass fin in the supporting structure.
- The coefficient of fixing *(n)* changes during testing, due to the changing supporting conditions caused by the continuous compression of the elastic damping material during loading.
- The calculation methods of the critical buckling force do not distinguish between float and heat-strengthened (HSG) glass.
- *Euler's* formula should be applied only in the case of float, monolithic single layer glass.
- The critical buckling force with *Sattler*'s formula overestimates the experimental values in the case of laminated glass consisted of float glass and gives correct values in the case of laminated glass consisted of HSG glass.
- The critical buckling force with *Allen*'s and *Zenkert*'s formulae result the same, usually lower, conservative values compared to the experimental results.
- In the case of conservative engineering calculations the use of *Blaauwendraad*'s formula is suggested.

b) The following conclusions can be drawn based on the laboratory experiments [1]:

- Three different stages can be distinguished in the buckling behaviour of glass columns.
- The buckling behaviour is not affected by the loading rate in the case of loading rate of 0.5 mm/min and 1mm/min.
- The critical buckling load is reduced with the increase of the number of glass layers.
- The allowed buckling load during structural design calculations is suggested to be the maximum load of the 1st Stage (stable state) reduced with safety factors.
- The 2nd Stage in the buckling behaviour is mainly influenced by the type of the supporting structure (fixed/pinned) and the stiffness of the glass columns.
- In the case of laminated glass, the horizontal deformations and the load bearing capacity are influenced by the shear modulus of the interlayer material, therefore the force in the 3rd Stage decreases.
- In the case of a single layer HSG glass with height of 1000 mm the critical buckling force increased with ~30% compared to that of float glass.

6. Acknowledgement

Authors express their gratitude to Rákosy Glass Ltd. for providing the specimens. Authors are thankful to the Department of Construction Materials and Engineering Geology, BME and *Mr. András Eipl* (Struktúra Kft) and *Mr. Péter Molnár* (Struktúra Kft) for their technical support.

References

[1] Nehme, K. – Jakab, A. – Nehme, S.G.: Experiments on the buckling behaviour of glass columns. Part 1. *Építőanyag*, 65. évf. 3. szám (2013), pp. 62–66. http://dx.doi.org/10.14382/epitoanyag-jsbcm.2013.13

[2] Pankhardt, K.: Load bearing glasses. Testing of construction glasses, Saarbrücken: Lap Lambert, 2012. -ISBN: 978 3 8473 2191 0

[3] Nehme, K. – Nehme, S. G. – Jakab, A.: Üveg oszlopok kihajlása, (Buckling of glass columns) Műszaki Tudomány az Észak-Kelet Magyarországi Régióban 2013, Konferencia előadásai, szerkesztette: Pokorádi L., DE MK, 2013. június 4., *DAB Műszaki Szakbizottsága*, Debrecen, 2013, ISBN 978-963-7064-30-2, pp. 378-388.

[4] Allen, H.G.: Analysis and Design of Structural Sandwich Panels, *Pergamon*, Oxford. UK, CH.8. 1969.

[5] Sattler, K. – Stein, P.: Ingenieurbauten 3, Theorie und Praxis, *Springer-Verlag*, Wien 1974.

[6] Zenkert, D. (editor): The Handbook of Sandwich Construction, *Engineering Materials Advisory Service Ltd*, Cradley Heath, West-Midlands, United Kingdom 1997.

[7] Blaauwendraad, J.: Buckling of laminated glass coloumns, *Heron*, Vol. 52, No. 1/2, 2007, pp.147-164.

[8] Wölfel, E.: Nachgiebiger Verbund eine Näherungslösung und deren Anwendungs-möglichkeiten, *Stahlbau*, No.6, 1987, pp.173-180.

Ref.:
Kinga **Nehme** – András **Jakab** – Salem Georges **Nehme**: *Experiments on the buckling behaviour of glass columns. Part 2.*
Építőanyag, 65. évf. 4. szám (2013), 112–117. p.
http://dx.doi.org/10.14382/epitoanyag-jsbcm.2013.21

Üvegoszlopok kihajlásának laboratóriumi vizsgálata. 2. rész.

Korábbi cikkünkben [1] laboratóriumi kísérleteink alapján ismertettük a teherhordó üveg oszlopok kihajlási viselkedését, valamint vizsgáltuk az üveg oszlopok teherbírási kérdéskörét. Jelen cikkünkben szintén a teherhordó üveg oszlopokkal foglalkozunk, a meglévő számítási eljárásokkal meghatározzuk a kritikus terhet, elemezzük a stabilitási viselkedést. Összehasonlítjuk a kísérleti és elméleti számítások eredményeit. Eredményeink tükrében elemezzük a nemzetközi irodalomban fellelhető számítási eljárásokat. A BME Építőanyagok és Mérnökgeológiai Tanszék laboratóriumában kísérleti úton vizsgáltuk az üveg oszlopok kihajlását. Több mint 60 db próbatestet tönkremenetelig terheltünk. Kísérleti eredményeink alapján meghatároztuk a kritikus erőt, erő-alakváltozás diagramokkal szemléltettük a tönkremeneteli és stabilitási folyamatokat. A kritikus teher és karcsúság összefüggését meghatároztuk, monolitikus (egy rétegű) és többrétegű üvegekből felépülő üveg oszlopok esetére.
Kulcsszavak: üveg oszlop, kihajlás, teherbíró üveg, stabilitás, átlátszóság

Simple basic model for concrete and its application

Part 3. Factors affecting consistency, material balance equations and mix design

Gyula PEKÁR ▪ private consultant ▪ alba-qualit@hdsnet.hu

Érkezett: 2013. 06. 06. ▪ Received: 06. 06. 2013. ▪ http://dx.doi.org/10.14382/epitoanyag-jsbcm.2013.22

Abstract

During the plant observations a number of interesting questions arose concerning consistency. The manufacturing plants (or the sites where pre-mixed concrete is transported from) are the ideal place for carrying out investigations to gather a wealth of valuable data. Nevertheless, the statistical characteristics for consistency in no way demonstrate the same kind of close correlation as those for compressive strength or deformation, so there is justification in being cautious, even though being cautious should never prevent us from drawing certain conclusions. When designing the composition of fresh concrete mixes, it may be useful to incorporate the (structural) content indicators of the concrete composition, provided that we know (or conduct experiments to find out) the correlations between the concrete composition content indicators and the properties of the fresh and hardened concrete, and apply the material balance equations of concrete mixes. The final part in this series of papers focuses on these issues.

Gyula PEKÁR

Chemical engineer (University of Veszprém, 1981). Active in the construction industry since 1984, first as a research engineer, and later as head of the laboratory at ARÉV, which was at the time the leading construction company in Székesfehérvár. From 2000, as a private consultant, he prepared enterprises for the implementation and operation of a number of QA systems (ISO 9001, ISO 14001, ISO/IEC 17025). From 2007-2013 he was a part-time engineering inspector at the state-owned ÉMI (Non-Profit Limited Liability Company for Quality Control and Innovation in Building). With the support of ÉMI, he carried out a research project, originally in conjunction with the Augusztin Concrete Manufacturing Company (Zamárdi), to establish the correlations between concrete compositions and the performance indicators of the set concrete, by recording observations of concrete mixes during their manufacture at the mixing plant. In 2011, he was invited by the Hungarian Institute for Transport Sciences to participate in research into low-shrinkage floor concrete compositions.

1. A brief review of the literature

A knowledge of the factors that affect the consistency of fresh concrete is important for conscious planning of *workability*, and research has therefore long been conducted into this area. The work of *Alexanderson* is especially interesting because he has examined the different *composition* conditions under which constant consistency (consistency of the same class) can be provided, across a very *broad range* of mixes, from *paste* (mortar) *mixes* to *concrete mixes* [1]. The diagrams he published (see *Figs. 27* and *28*) express the principle that consistency could only remain constant when *dry* aggregates are added to a given cement paste of a known consistency if the water-cement ratio is simultaneously increased. The volumetric ratio of the aggregates in the concrete, however, can only be increased to a maximum limit, which also depends on consistency, roughly in line with *Fig. 28*. *Alexanderson* is remarkable in that he not only considers the *air content* of pastes (admixtures which form bubbles of air) and the impact they have on consistency, but he also calculates with it.

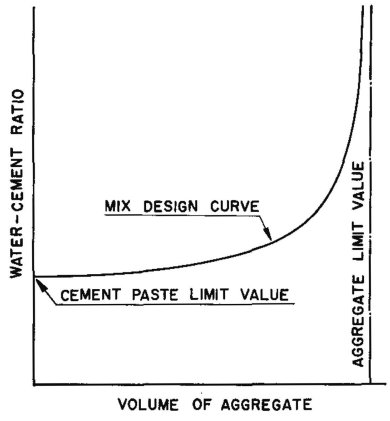

Fig. 27. Relationship between the percentage of aggregate by volume and the water/cement ratio at constant consistency, after Alexanderson [1]

27. ábra Az azonos konzisztencia biztosításához szükséges v/c tényező változása a betonban levő adalékanyag térfogatarányának függvényében, Alexanderson szerint [1]

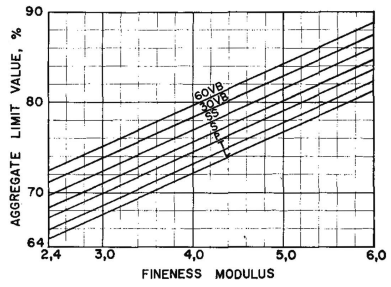

Fig. 28. Aggregate limit value for concrete made with natural coarse aggregate and air content 1.5-2.5 V% (the Swedish designations for consistency classes are roughly in line with the scale of S1…S4 consistency classes)

28. ábra Az adalékanyag bedolgozható maximális térfogatarányának függése a finomsági modulustól, különböző konzisztencia-osztályok esetén (a svéd jelölések fentről lefelé nagyjából az S1…S4 osztályoknak felelnek meg)

In Hungary, the work of *Ujhelyi* in mix design accounting for consistency is outstanding: his DSc thesis of 1989 [2] not only gives a thorough summary of the methods for estimating water demands, but also describes a new method for calculating consistency-dependent water demands. The method is suitable for the design of consistency of mixes *without admixtures*. In the proposed formulae the water demands of aggregates depend on the *fineness modulus*, and the water demands of cement depend on the *specific surface area*. The latter predicts the so-called *surface aspect*: it is noticed that not only the masses and volumes of the set of solid phase components are included in concrete mixes, but also their *surface areas*, and the surface areas may have particular influences on the properties of the concrete.

Design of consistency is complicated due to the presence of cements and additions which have high specific surface areas and by the effects of high range water reducing admixtures - which can produce special rheological phenomena. This is the reason behind the ever increasing number of articles published in the last decade that deal with observations of the rheological behaviour of cementitious mixes. In Hungary, *Spránitz* and his associates have examined the *flow time* and *flow value* of pastes made by different

cements and admixtures, and have found numerical correlations between the rheological properties and the composition properties [3,4]. Their work was consciously directed towards the investigation of *pastes*, since (as *Alexanderson* also recognised) the rheological behaviour of concrete is determined to a great extent by the properties of the paste.

A source of inspiration for future research in Hungary could be provided by the report of *Toutou* and *Roussel* [5]. The authors examined the rheological behaviour of concrete constituents in *four cumulative* stages: firstly *in suspensions* (water + silica fume), secondly *in pastes* (water + silica fume + cement), thirdly *in mortars* (water + silica fume + cement + sand), and fourthly *in concretes* (water + silica fume + cement + sand + gravel). The rheological properties of all four types of mixes were investigated, and they reported interesting data concerning the correlations between *shear stress* and *shear rate*, and between *yield stress* and combined *volumetric ratios of solid phase constituents*. It would be worth pursuing this direction of research in Hungary too; it would not require unaffordable costs, but mainly systematic and perseverant work. The outcome would be more reliable mix design for concrete workability, particularly in the case of high performance concretes, which are more sensitive from a rheological point of view.

2. Factors influencing consistency according to the simple basic model for concrete

In the simple basic model, the influence of *concrete composition content indicators* is also a *subject for analysis* with regard to consistency and the rheological properties of fresh concrete (*p*: ratio of paste in the concrete, *x*: volumetric ratio of liquid to paste powder, χ_c: volumetric ratio of cement in the paste powder, λ_{AD}: volumetric ratio of admixtures to paste powder, *l*: volumetric ratio of air in the concrete), although the *physical properties of concrete constituents* must be considered at all times. For example, one such important influencing factor is the *volumetric specific surface area* of the *combined solid phase matter (paste powder and aggregate particles)* making up the concrete, which is calculated by the method described in [6]; which is essentially the procedure proposed by *Kausay* [7], with the difference that *as standard* the particles are considered to be not spherical, but ellipsoid in shape. The role of the surface area of materials included in concrete mixes is obvious, because during the flow of the concrete, the *combined solid particles have a mutual effect on each other through their surface areas*, and also have an effect on the fluid (*water*, which may also contain *admixtures)* that plays the role of dispersing agent.

Concrete is considered from a rheological point of view to be a self-affine (fractal-like) composite system, which manifests itself in the combined solid phase of constituents in dimensions of different scales *showing a repeating structure*. The *cement + addition powder* as *dispersed phase* plays the same role *in paste* as it is played by *aggregate in concrete*. Also, the *fluid* (mostly water), which is the *dispersing agent* in the paste plays the same role as it is played by the *paste in concrete*. *Paste* acts as the *dispersing agent* for the *aggregate* as the *dispersed phase*. The only substantial difference between the aforementioned dispersed phases lies in the *2 order of magnitude* difference between their particle sizes, but the structure in the different magnitude scales is *continuously* repeated, which can presumably be traced back to the *exponential distribution* of the particle sizes of the combined solid phase constituents of concrete.

If the surface of the powder particles of the paste are covered in a *thick layer* of fluid (but naturally not so thick that they can bleed) then the paste can be expected to flow better than if the layer of fluid covering the particles is *thinner*. The same large-scale range of dimensions is still valid: if the surface of the aggregate is covered by a *thick layer* of paste (acting almost as a fluid) then the fresh concrete mix can be expected to flow better than in the case where the aggregate gets a *thin layer* of paste. From the point of view of fluidity, *the consistency of the neat paste serves as the maximum threshold value* (in this case the *paste thickness* is infinite), since when combined solid phase matter is added to the paste (either aggregate or paste powder) then the added surplus surface area dilutes the thickness of the dispersing agent covering the dispersed particles, causing a decreased fluidity of the mix.

The influence of water-reducing admixtures ($\lambda_{AD} > 0$) – following the above idea – can also be interpreted as diluting the thicknesses of the dispersing agent which would be necessary to achieve a given consistency in mixes without admixtures *in every range of dimensions of the dispersed phase particles*. In the case of the 132 batches of plastic consistency concrete mixes investigated during the *plant observations* detailed in [8] (of which 72 were made without admixtures, and 60 were made by water-reducing admixture), the *average thickness* of the paste (as dispersing agent) reaching the aggregates within the range of dimensions ∅0.063-32 mm was, significantly, *several μm thinner* for mixes *with* admixtures than for mixes *without* admixtures. This paste diluting effect can actually represent savings in paste between 10 to 30 litres (depending on the type and characteristics of the aggregate) when applied to each cubic meter of mix.

If the mix composition of the concrete is known, then the *thickness* of a dispersing agent covering a *d* sized particle in the dispersed phase can be calculated simply by Eqs. (37) and (38):

$$t_a = \frac{1}{2} \cdot d_a \left(\left(1 + \frac{p}{a} \right)^{\frac{1}{3}} - 1 \right) \tag{37}$$

$$t_z = \frac{1}{2} \cdot d_z \left((1 + x)^{\frac{1}{3}} - 1 \right) \tag{38}$$

where:

t_a is the thickness [mm] of the layer of paste covering the *aggregate* particles of diameter d_a [mm],

t_z is the thickness [μm] of the layer of fluid (water) covering the *paste powder* particles of diameter d_z [μm],

p is the volumetric ratio of the paste in the concrete (concrete composition content indicator),

a is the volumetric ratio of aggregate in the concrete (a>0), and

x is the volumetric ratio of fluid-paste powder.

		Concrete composition (structural) content indicators					Other technical data and information			
		p	x	χ_c	λ_{AD}	l	Admixtures included in the evaluation*	Traditional w/c ratio	a**	D_{max} mm
Plant observations of consistency 2008-2010. 242 observations	min	0.153	0.924	0.552	0.000	0.000	High range water reducer (HRWR)	0.335	0.652	4
	max	0.314	3.381	0.977	0.030	0.088		1.218	0.790	32
	average	0.255	1.684	0.839	0.009	0.017	Mid range water reducer (MRWR) and	0.685	0.728	24
	distribution	0.021	0.301	0.080	0.009	0.014	3 types of water reducers (WR)	0.143	0.019	8

*Table 11. Concrete composition content indicators and other data for mixes subjected to consistency examinations during plant observations; *Note: The product names of the admixtures have been omitted intentionally; **Note: a: the volumetric ratio of aggregate in the concrete mix*

11. táblázat Az üzemi megfigyelések során konzisztencia-vizsgálatoknak alávetett keverékek betonösszetételi állapotjelzői és egyéb adatai (az adalékszerek termékmegnevezéseit szándékosan mellőzzük, ** a: a betonkeverékben lévő adalékanyag térfogataránya)*

Admixture code name	Number of observations	*p* – paste volumetric ratio		x - fluid-powder volumetric ratio		λ* - dose of admixture as *volumetric ratio* of the paste powder			Measured flow values [mm]		Factors for Eq. (39)	
		p_{min}	p_{max}	x_{min}	x_{max}	λ_{min}	$\lambda_{average}$	λ_{max}	$flow_{min}$	$flow_{max}$	$f_{1,AD}$	$f_{2,AD}$
without admixture	113	0.153	0.302	1.254	3.381	0.000	0	0	300	470	1	1
HRWR	49	0.220	0.267	1.287	1.675	0.010	0.014	0.025	390	550	14.256	1.004
MRWR	10	0.212	0.314	0.924	1.872	0.008	0.016	0.030	340	590	8.868	1.012
WR-1	28	0.214	0.285	1.076	1.975	0.012	0.020	0.029	380	480	4.529	1.012
WR-2	31	0.217	0.290	1.297	1.876	0.006	0.016	0.028	350	480	4.846	1.017
WR-3	11	0.240	0.263	1.215	1.850	0.012	0.020	0.028	390	480	4.042	1.004

Table 12. Data concerning the concrete composition content indicators and consistency values for mixes made with and without different types of admixture, and the factors $f_{1,AD}$ and $f_{2,AD}$ of Eq. (39)

12. táblázat Az adalékszer nélküli és a különböző adalékszerekkel megvalósult keverékek betonösszetételi állapotjelzőinek és konzisztencia mértékszámainak adatai, valamint a (39) képlet $f_{1,AD}$ és $f_{2,AD}$ faktorai

What the above formulae express is, in essence, that the thickness of the dispersing agent is *directly* proportional to the *size of the particles* in the dispersed phase, and the proportionality ratio depends on the volumetric ratio of the dispersing agent and the dispersed phase. One of the tasks of a concrete engineer in connection with this topic is to determine – for concrete constituents – the volumetric ratio that achieves the optimum dispersing agent thickness in relation with the distribution of the dimensions of solid particles, in order to reach the targeted consistency.

3. Results and evaluation of plant observations

3.1. General data

Consistency was measured by the flow table test acc. to EN 12350-5 within 15±5 minutes of the start of mixing the concrete. The compositional properties of the mixes examined were hardly altered from those described in *Table 5* of [6], although the database had been updated with the data from new mixes. The current data is summarised in *Table 11*. More detailed data on the concrete composition content indicators of the mixes prepared with admixtures are summarised in *Table 12*. It can be realised from the data in *Table 12* that the mixing plant produced an overwhelming majority of concrete mixes of F2 and F3 consistency according to EN 206-1, according to its customer orders.

A general presentation of the data would be incomplete without showing the range limits of the variations in *particle distributions* of the mixes of sand and gravel fractions. The distribution curves of all aggregate mixes have been condensed into the single diagram in *Fig. 29*, which shows the distribution according to the *surface area pass* calculated for the unit of volume rather than the volume or mass percentage pass. It can be seen that there are considerable differences in the volumetric specific surface areas over 0.5 mm particle size, changing between 4000-6000 m^2/m^3. The influence of the volumetric specific surface area is, therefore, expected to be a major factor when considering the consistency of the mixes.

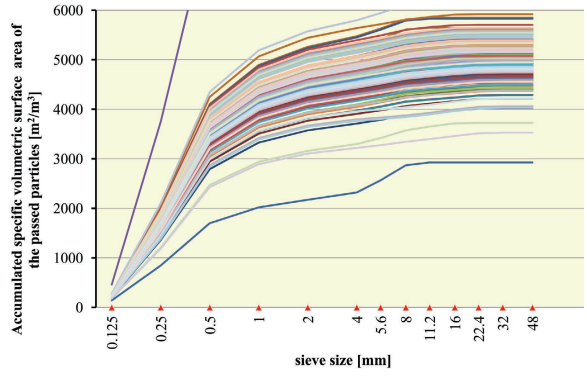

Fig. 29. Surface area distribution of aggregate mixes used between 2008-2011 (the single curve that leaves the chart is for sand with a volumetric specific surface area of ~12 000 m^2/m^3)

29. ábra A 2008-2011 között felhasznált adalékanyag-keverékek felületeloszlásai (az ábrából kifutó egyetlen görbe egy ~12 000 m^2/m^3 térfogati fajlagos felületű homokhoz tartozik)

3.2. Relationship between consistency and concrete composition content indicators

In processing the results of the observations, correlations were initially sought in the data of *mixes made without admixtures*, and the basic equations derived from the analysis were later used for compositions containing admixtures to calculate *factors* that expressed the effects of the admixtures. The equation that was found to match most closely the observed measured results is shown in Eq. (39).

$$Flow\,[\mathrm{mm}] = \left(1 + f_{1,AD} \cdot \lambda_{AD}\right) \cdot f_{2,AD} \cdot A \cdot \frac{\left(\frac{x}{f_z}\right)^{n_x}}{\left(1 + \frac{a \cdot f_a}{z \cdot f_z}\right)^{n_f} \cdot \left(1 + \frac{a}{z}\right)^{n_a}} \quad (39)$$

where:

Flow is the estimated flow value [mm] of the concrete mix by flow table,

λ_{AD} is the dose of admixture in the volumetric ratio of paste powder (concrete composition content indicator),

$f_{1,AD}$ is the *dose factor* of the admixture (for specific values of the observed admixtures, see *Table 12*),

$f_{2,AD}$ is the factor typical of the *material* of the admixture (for specific values of the observed admixtures, see *Table 12*),

A is the experimental constant, in this case A=39386.8,

n_x, n_f and n_a are exponents, with observed values as follows: n_x=0.288, n_f=1.208 and n_a=0.319,

f_z is the volumetric specific surface area of the paste powder [m^2/m^3],

f_a is the volumetric specific surface area of the aggregate [m^2/m^3],

z is the volumetric ratio of paste powder in the concrete,

a is the volumetric ratio of aggregate in the concrete, and

the other notations are the same as for Eqs. (37) and (38).

The correlation is quite *weak* ($R^2 \approx 0.29$), which is not surprising in the case of consistency, but the significance of the equation's multiplication factor was proved with a probability of p=0.06. The confidence interval for the flow values obtained from estimates was ± 88 mm at a probability level of 95% and ± 36 mm at a probability level of 67%. An interesting feature of the relationship is that when a=0 (that is, for pure paste) it assumes the *maximum value*, which complies with the principles defined by *Alexanderson*. What is new is that it also takes into account the influence of the dose of admixture (λ_{AD}), as well as its *effectiveness* ($f_{1,AD}$) and the influence of its type ($f_{2,AD}$). For the latter, a value that very closely approaches unity was obtained during the plant observations (see *Table 12*). Where mixes without admixture are concerned, the equation gives the estimated flow values for mixes with only water added, since $f_{1,AD} = f_{2,AD} = 1$ if λ_{AD}=0.

The flow values estimated from Eq. (39) must be regarded as *expected* values, which can assume any value within the confidence interval given above, but the calculated values are the *most probable (expected)* values. A few illustrations from processing the results are shown in *Figs. 30* to *33*. It can be realised from *Fig. 33* that for a given w/c range and paste

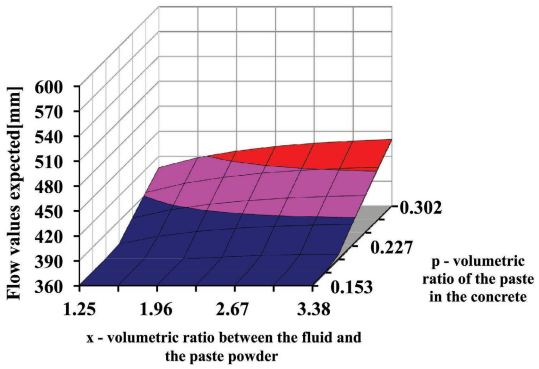

Fig. 30. Expected flow values for mixes made without admixture (λ_{AD}=0) in the observed p-x range

30. ábra Adalékszer nélküli (λ_{AD}=0) keverékek terüléseinek várható értékei a megfigyelt p-x tartományban

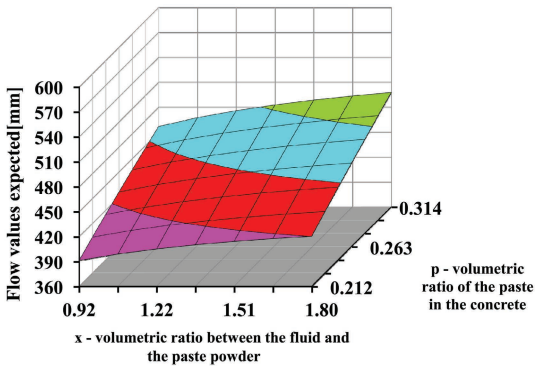

Fig. 31. Expected flow values for medium (λ_{AD}=0.016) doses of MRWR admixture in the observed p-x range

31. ábra Erős hatású adalékszer (MRWR) közepes (λ_{AD}=0,016) adagolása mellett elérhető terülések várható értékei a megfigyelt p-x tartományban

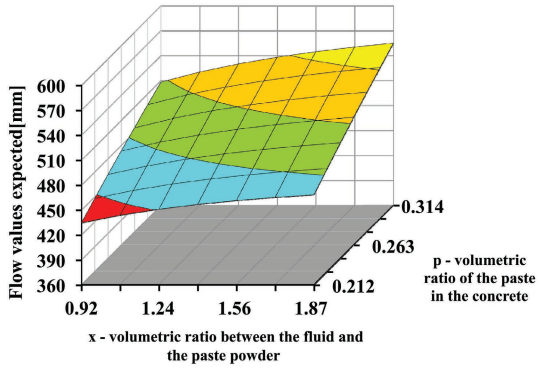

Fig. 32. Expected flow values for high (λ_{AD}=0.030) doses of HRWR admixture in the observed p-x range

32. ábra Nagyon erős hatású adalékszer (HRWR) magas (λ_{AD}=0,030) adagolása mellett elérhető terülések várható értékei a megfigyelt p-x tartományban

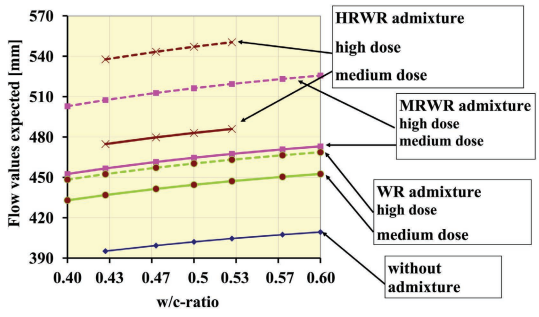

Fig. 33. Consistencies obtained with different admixtures, and without admixtures, depending on dosage, in the case of concrete mixes with a paste content of 280 l/m³, air content of 20 l/m³, and no additions

33. ábra A különböző adalékszerekkel, és azok nélkül elérhető konzisztenciák az adagolás függvényében 280 liter/m³ péptartalmú, 20 liter/m³ levegőtartalmú, kiegészítőanyagot nem tartalmazó betonkeverékek esetén

content, a high dosage of the medium range admixture may perform almost identically to a medium dosage of high range admixture. Increasing the dosage of admixture within a certain limit is a more significant influence than increasing the w/c ratio.

4. Material balance equations of concrete mixes

According to the definition given in the EN 206-1 European Standard concrete is a "material formed by mixing cement, coarse and fine aggregate and water, with or without the incorporation of admixtures, additions or fibres, which develops its properties by hydration" [9]. In addition to this definition – taking account of recent developments in the field of concrete engineering – the simple basic model for concrete mixes also regards concrete in its fresh state as a *macroscopically heterogeneous composite system* consisting of *solid phase (aggregates)*, *liquid phase (paste)* and *gaseous phase (air)*, in which the *paste* is itself a heterogeneous system, likewise consisting of *three* separate phases, which are:

- solid phase *paste powder* (cement, as a hydraulic bonding agent, perhaps together with (a mixture of) fine-grain *additions*, which are inert or have pozzolanic reactivity, latent hydraulic reactivity, etc.),
- liquid phase *water* (which may also contain one or more dissolved *admixtures*) and
- gaseous phase *air* (which may be intentionally added air bubbles by air entraining admixture, or just randomly remaining voids due to incomplete compaction).

A $V_{concrete}$ [m³] volume of (fresh) concrete mix generally consists of five *main* concrete constituent components, while certain concrete constituents may themselves be made up of mixtures of sub-constituents (in known proportions):

K_{virt}*[kg]: total additions; $K_{virt} = \Sigma(\alpha_{M,Kvirt,i} K_{virt,i})$, where $\alpha_{M,Kvirt,i}$ is the *mass ratio* of the i^{th} $K_{virt,i}$ [kg] addition component, and where $0 \le \alpha_{M,Kvirt,i} \le 1$ and $\Sigma\alpha_{M,Kvirt,i} = 1$,

c [kg]: quantity of cement added,

AG_{virt}*[kg]: total (wet) aggregates; $AG_{virt} = \Sigma(\alpha_{M,AGvirt,j} AG_{virt,j})$, where $\alpha_{M,AGvirt,j}$ is the *mass ratio* of the j^{th} $AG_{virt,j}$[kg] aggregate component, and where $0 \le \alpha_{M,AGvirt,j} \le 1$ and $\Sigma\alpha_{M,AGvirt,j} = 1$,

W_{virt}*[kg]: quantity of water *added when blending the concrete mix*,

AD [kg]: total admixtures; $AD = \Sigma(\alpha_{M,AD,k} AD_k)$, where $\alpha_{M,AD,k}$ is the *mass ratio* of the k^{th} AD_k [kg] admixture component, and where $0 \le \alpha_{M,AD,k} \le 1$ and $\alpha_{M,AD,k} = 1$.

*Note: the "virt" (virtual) symbol used above expresses that parts belonging to the *different phases* of the concrete are (or may be) present in the concrete constituent components. For example, the part of the addition material which is *larger than* 0.063 mm is included in the solid phase of the aggregate, while the part of the aggregate which is *smaller than* 0.063 mm is included in the fluid paste as paste powder. The water which adheres to the surface of the aggregate, and which in many cases is not negligible, is also included in the paste – as a liquid – so in addition to the W_{virt} added water, this must also be taken into consideration in the liquid phase of the concrete.

The *structural composition* of concrete mixes described by the *mass data* above may also be basically described using *five* dimensionless ratios:

p: the volumetric ratio of paste in the concrete ($0 < p \le 1$),

x: the volumetric ratio of the (free) liquid and the paste powder in the paste ($x > 0$, but generally in practice: $\sim 0.6 \le x \le \sim 3.6$),

l: the volumetric ratio of air (void) in the concrete ($0 \le l < 1$, generally in practice: $\sim 0.010 \le l \le \sim 0.060 \ldots 0.120, \ldots$),

χ_c: the volumetric ratio of cement in the paste powder ($0 < \chi_c \le 1$, if the paste is pure cement $\chi_c = 1$),

λ_{AD}: the *combined* volumetric ratio of the admixture compared with the paste powder, (where the $\lambda_{AD,k}$ ratios of individual – different effect – admixture components are $\lambda_{AD,k} \ge 0$, where the concrete mix contains no admixture $\lambda_{AD,k} = 0$; in general, however, $\lambda_{AD,k} = \sim 0.005 \ldots 0.050$, and is therefore a small value).

The correlations between the concrete composition content indicators and the amounts of the given concrete constituents with known physical properties are defined by the system of linear equations in the matrix equation shown in Eq. (40), where:

$\varphi_{K,i}$: the part of the i^{th} addition component which is smaller than 0.063 mm, as mass ratio,

$\rho_{K,i}$[kg/m³]: the dried particle density of the i^{th} addition component,

ρ_c[kg/m³]: the particle density of the cement (in dry state),

$\varphi_{AG,j}$: the part of the j^{th} aggregate component which is smaller than 0.063 mm, as mass ratio,

$w_{AG,j}$: the moisture content of the j^{th} aggregate component as mass ratio,

$$\begin{pmatrix} \sum_{i=1}^{n_K} \alpha_{M,Kvirt,i} \cdot \frac{\varphi_{K,i}}{\rho_{K,i}} & \frac{1}{\rho_c} & \sum_{j=1}^{n_{AG}} \frac{\alpha_{M,AGvirt,j}}{1+w_{AG,j}} \cdot \frac{\varphi_{AG,j}}{\rho_{AG,fine,j}} & 0 & \sum_{k=1}^{n_{AD}} \alpha_{M,AD,k} \cdot \left(\frac{1}{\rho_{AD,k}} - \frac{1-sz_k}{\rho_w} \right) \\ -\frac{\sum_{i=1}^{n_K} \alpha_{M,Kvirt,i} \cdot sw_{K,i}}{\rho_w} & -\frac{sw_c}{\rho_w} & \sum_{j=1}^{n_{AG}} \frac{\alpha_{M,AGvirt,j}}{1+w_{AG,j}} \cdot \frac{w_{AG,j} - sw_{AG,j}}{\rho_w} & \frac{1}{\rho_w} & \sum_{k=1}^{n_{AD}} \alpha_{M,AD,k} \cdot \frac{1-sz_k}{\rho_w} \\ \sum_{i=1}^{n_K} \alpha_{M,Kvirt,i} \cdot \frac{1-\varphi_{K,i}}{\rho_{K,i}} & 0 & \sum_{j=1}^{n_{AG}} \frac{\alpha_{M,AGvirt,j}}{1+w_{AG,j}} \cdot \frac{1-\varphi_{AG,j}}{\rho_{AG,coarse,j}} & 0 & 0 \\ 0 & \frac{1}{\rho_c} & 0 & 0 & 0 \\ 0 & 0 & 0 & 0 & \sum_{k=1}^{n_{AD}} \frac{\alpha_{M,AD,k}}{\rho_{AD,k}} \end{pmatrix} \cdot \begin{pmatrix} K_{virt} \\ c \\ AG_{virt} \\ W_{virt} - \Delta W_{ev} \\ AD \end{pmatrix} = \begin{pmatrix} \frac{p}{1+x} \cdot V_{concrete} \\ \frac{p}{1+x} \cdot x \cdot V_{concrete} \\ (1-p-l) \cdot V_{concrete} \\ \chi_c \cdot \frac{p}{1+x} \cdot V_{concrete} \\ \sum_{k=1}^{n_{AD}} \lambda_{AD,k} \cdot \frac{p}{1+x} \cdot V_{concrete} \end{pmatrix} \quad (40)$$

$\rho_{AG,j,\,fine}$[kg/m³]: the dried particle density of the part of the j^{th} aggregate component which is smaller than 0.063 mm,
$\rho_{AD,k}$[kg/m³]: the density of the k^{th} admixture component,
sz_k: the dry content of the k^{th} addition component, as mass ratio,
ρ_w[kg/m³]: water density,
$sw_{K,i}$: (short-term) water absorption of the i^{th} addition component, as mass ratio,
sw_c: (short-term) water absorption of cement, as mass ratio,
$sw_{AG,j}$: (short-term) water absorption of the j^{th} aggregate component, as mass ratio,
$\rho_{AG,j,\,coarse}$[kg/m³]: the dried particle density of the part of the j^{th} aggregate component which is larger than 0.063 mm,
ΔW_{ev} [kg] the water that evaporates from the concrete mix with a volume $V_{concrete}$ [m³] *until it is worked in*,
$\lambda_{AD,k}$: the ratio of the volume of the k^{th} admixture component compared with the volume of the paste powder,
the other notations are the same as previously explained.

The system of linear equations presented in the matrix equation of Eq. (40) is fundamental in the mix design, determining the composition of concrete mixes. The system of equations expresses the fact that *(fresh) concrete mixes are made up of a linear combination of the constituent phases of components*. The *matrix* factor that may be regarded as *known* in the product on the *left hand side of the equation* (*materials property matrix*) contains the *physical properties and compositional proportions* (e.g.: fraction ratios) of the concrete constituent materials, while the *vector* factor of the product (*mix composition vector*) expresses the masses of the concrete constituents which are *to be added* - and which may be regarded as *unknown* during mix design. The so-called *structural vector* on the *right hand side of the equation* contains the volumes of paste powder, paste fluid and aggregates in a designed volume of concrete, as well as the volume of cement and the volume of the admixtures, respectively. The structural vector directly depends on the targeted concrete composition content indicators, which are either *already known* during mix design, or are *determined* on the basis of prior knowledge of particular correlations.

The *mix composition vector* and the *structural vector* mutually define each other in a clear way, so the design of the composition of concrete mixes is possible by solving the matrix equation of Eq. (40). During concrete mix design for a volume $V_{concrete}$, the first step is to *determine* the *concrete composition content indicators*, from which the *structural vector* on the right hand side of the matrix equation of Eq. (40) can be obtained. The matrix equation of Eq. (40) can be set up by the *materials property matrix* that contains the material properties and particular component proportions. The solution of the system of linear equations provides the *mix composition vector*, which produces, as a direct result, the quantities of the concrete constituents that are to be added to the targeted concrete mix with a volume $V_{concrete}$.

It should be noted that Eq. (40) (and therefore the concrete mix) may only be clearly defined *if all the concrete composition content indicators are known*. It also follows that *fully comprehensive* consequences can in theory only be drawn from observations related to concrete mixes, if the influence of *each* concrete composition content indicator has been taken into account and evaluated.

5. Using the simple basic model to design the composition of concrete mixes to meet given criteria

Several concrete mix design methods are available which meet pre-defined criteria. The common principle behind the different methods is to search for compositions which meet the criteria by *counting back from the design criteria* (e.g. compressive strength and consistency), which assumes that accepted correlations are available, as is the case with the *Palotás-Bolomey* [10,11] and *Ujhelyi* [2] methods used widespread in Hungary for *concretes without admixtures*.

New correlations are necessary for concrete mix design *with admixtures*. The simple basic model for concrete mixes provides this opportunity: the use of *material balance equations* is included, and greater flexibility in applying correlations with a *restricted range of validity* in connection with the influences of factors is offered; that are developed through *experiments*.

In the followings, a specific example illustrates the essence of the method.

6. Example for concrete mix design

The present example details the steps of concrete mix design by the simple basic model for a concrete mix with designation C30/37-XC3-16-F4-MSZ 4798-1:2004.

6.1 Identifying and determining requirements

Compressive strength: The concrete in the example needs to have a *characteristic compressive strength* of $f_{ck,cube}$ according to MSZ EN 206-1 standard that lies between the *minimum* values for compressive strength prescribed for compressive strength classes C30/37 and C35/45, i.e. 37 N/mm² ≤ $f_{ck,cube}$ <45 N/mm². It is possible to ensure the *characteristic compressive strength* in *continuous production* if the *mean compressive strength* of the concrete meets the condition of $f_{cm} \geq f_{ck,cube}+1.48\times\sigma$, where $\sigma \geq 3$ N/mm² is acceptable in the example. The estimate for the standard deviation of a population is recorded at 10% of the expected *mean* compressive strength of the concrete in the example, and the range of *values for characteristic compressive strength* is *narrowed* by 10% at both the upper and lower limits for safety reasons (which results 37.8 N/mm² ≤ $f_{ck,cube}$ <44.2 N/mm²). The achieved result safely fulfil the given conditions for compressive strength if the *mean compressive strength* lies in the range 44.4 N/mm² ≤ f_{cm} <51.9 N/mm².

Consistency: The flow value [mm] prescribed for consistency class F4 according to MSZ EN 206-1 standard lies in the range 490 mm ≤ *Flow* ≤ 550 mm. In view of the uncertainties in estimating consistency, the range midpoint of *Flow*=520 mm has been taken as the criterion.

Composition criteria: The recommendations according to MSZ EN 206-1 standard for exposure class XC3 are $w/c \leq 0.55$ and $c \geq 280$ kg/m³. Further requirements in Hungary are the minimum body density of fresh concrete of 2380 kg/m³ and the minimum body density of hardened concrete of 2310 kg/m³.

Components of concrete		Mass ratios in constituents		volumetric specific surface	fine-content (<0.063 mm)		Dry densities		Moisture content		Absorption of water	
marking	name	marking	value	[m²/m³]	marking	[m%]	marking	[kg/m³]	marking	[m%]	marking	[m%]
W_{virt}	water						ρ_w=	999				
AD	MRWR admixture	$a_{M,AD,1}$=	1,000				$\rho_{AD,1}$=	1070	1-sz_1=	70,0%		
c	CEM II/A-M (V-LL) 42,5 N			f_c=1208000			ρ_c=	3000			sw_c=	1,51%
K_{virt}	inert basalt powder	$a_{M,Kvirt,1}$=	1,000	f_K=1456000	$\Phi_{K,1}$=	88,0%	$\rho_{K,1}$=	2763			$sw_{K,1}$=	0,50%
	$0/4_{virt}$	$a_{M,AGvirt,1}$=	0,451	9859	$\Phi_{AG,1}$=	0,4%	$\rho_{AG,fine,1}$= $\rho_{AG,coarse,1}$=		$w_{AG,1}$=	3,49%	$sw_{AG,1}$=	0,20%
AG_{virt}	$4/8_{virt}$	$a_{M,AGvirt,2}$=	0,280	1365 fa= 5034	$\Phi_{AG,2}$=	0,3%	$\rho_{AG,fine,2}$= $\rho_{AG,coarse,2}$=	2640	$w_{AG,2}$=	1,71%	$sw_{AG,2}$=	0,95%
	$8/16_{virt}$	$a_{M,AGvirt,3}$=	0,269	926	$\Phi A_{G,3}$=	0,2%	$\rho_{AG,fine,3}$= $\rho_{AG,coarse,3}$=		$w_{AG,3}$=	1,21%	$sw_{AG,3}$=	0,95%

Table 13. Data of the concrete constituents that are available for concrete with designation C30/37-XC3-16-F4-MSZ 4798-1:2004, which is to be designed in the example (note: sz_1 refers to dry content of the MRWR admixture)

13. táblázat A példa szerint tervezendő C30/37-XC3-16-F4-MSZ 4798-1:2004 jelű betonhoz rendelkezésre álló betonalkotók adatai

Type of cement taken into account	Content (stuctural) indicators					Other technical data		
CEM II A-M (V-LL) 42,5 N		p	x	χ_c	λ_{AD}	l	tradi-tional w/c	a*	D_{max} mm
Augusztin Betongyártó Ltd. 2008-2010. 46 observations	min.	0.204	1.294	0.750	0.010	0,000	0.484	0.686	8
	max.	0.302	2.327	0.974	0.026	0.041	1.048	0.756	32
	AVG.	0.261	1.753	0.822	0.019	0.012	0.729	0.727	24,5
	STD.	0.016	0.243	0.055	0.006	0.007	0.138	0.014	8

Table 14. Concrete composition content indicators and other data of CEM II/A-M (V-LL) 42.5 N mixes evaluated during industrial observations (a: volumetric ratio of the aggregate in the concrete mix)*

14. táblázat Az üzemi megfigyelések során értékelésbe vont CEM II/A-M (V-LL) 42,5 N keverékek betonösszetételi állapotjelzői és néhány más adata (a: a betonkeverékben lévő adalékanyag térfogataránya)*

Admixture code	Observations (no.)	*p* – paste volumetric ratio		*x* - liquid-powder volumetric ratio factor		λ - dose of admixture in the paste powder *volumetric ratio*			Measured Flow [mm]		Factors in the estimation formula	
		p_{min}	p_{max}	x_{min}	x_{max}	λ_{min}	λ_{AVG}	λ_{max}	$Flow_{min}$	$Flow_{max}$	$f_{1,AD}$	$f_{2,AD}$
MRWR	10	0.212	0.314	0.924	1.872	0.008	0.016	0.030	340	590	8.868	1.012

Table 15. Data on the concrete composition content indicators and consistency measurements of mixes made by mid-range water-reducing MRWR admixture, and the $f_{1,AD}$ and $f_{2,AD}$ factors of the consistency estimation formula of Eq. (42)

15. táblázat Az erős hatású adalékszerrel (MRWR) készített keverékek betonösszetételi állapotjelzőinek és konzisztencia mértékszámainak adatai, valamint a konzisztenciabecslő (42) képlet $f_{1,AD}$ és $f_{2,AD}$ faktorai

No	Target parameters and content inicators							Composition (for dry aggregates) kg/m³					Design composition (for wet aggregates) kg/m³							Checking		
	$f_{cm28,exp}$ [N/mm²]	$Flow_{exp}$ [mm]	p	χ_c	l	x	λ_{AD} (MRWR)	K	CEM II/ A-M 42.5	AG	W	AD_1 (MRWR)	stone powder	CEM II/ A-M 42.5	0/4 sand	4/8 gravel	8/16 gravel	W_{virt}	AD_1 (MRWR)	w/c	ρ_{fresh} kg/m³	expo-sure class
1	44,4	520	0,280	0,850	0,020	1,333	0,034	46	306	1849	173	4,32	46	306	853	530	509	129	4,32	0,54	2379	XC3
2	44,4	520	0,280	0,972	0,020	1,560	0,030	-0	319	1854	184	3,54	-0	319	856	532	510	140	3,54	0,55	2361	XC2
3	44,4	520	0,300	0,850	0,020	1,317	0,030	51	330	1795	184	4,11	51	330	829	515	494	141	4,11	0,53	2365	XC2
4	44,4	520	0,300	0,975	0,020	1,559	0,026	-0	343	1801	197	3,27	-0	343	831	517	496	154	3,27	0,55	2344	X0
5	51,9	520	0,280	0,850	0,020	1,183	0,036	50	327	1848	165	4,91	50	327	853	530	509	121	4,91	0,48	2395	XC4
6	51,9	520	0,280	0,973	0,020	1,408	0,032	-0	339	1854	177	3,96	-0	339	856	532	510	133	3,96	0,50	2375	XC3
7	51,9	520	0,300	0,850	0,020	1,168	0,032	55	353	1795	175	4,72	55	353	828	515	494	133	4,72	0,47	2382	XC3
8	51,9	520	0,300	0,976	0,020	1,396	0,028	-0	366	1801	189	3,72	-0	366	831	517	496	146	3,72	0,49	2360	XC2

Table 16. The composition calculations performed on the basis of the example criteria, where $f_{cm,28,exp}$ and $Flow_{exp}$ are the assumed design criteria (target parameters), p, χ_c and l are freely selected, and x, λ_{AD} are calculated content indicators dependent on the preceding. The Table contains the recipes derived from solving the matrix equation of Eq. (40), mixing instructions (for wet aggregate components) and a control column for the exposure requirements

16. táblázat A példa szerinti kritériumok alapján végzett összetétel-számítások, ahol az $f_{cm,28,exp}$ és $Flow_{exp}$ felvett tervezési kritériumok (célparaméterek), p, χ_c és l szabadon választott, az x, λ_{AD} pedig ezektől függő számított állapotjelzők. A táblázat tartalmazza a (40) egyenletrendszer megoldásából kapott receptúrákat, keverési utasításokat (nedves adalékanyag-komponensekre) és egy ellenőrző blokkot a kitéti követelményekre

6.2 Identifying the concrete constituent materials and determining their properties

The example does not take the quantity of evaporating water into consideration, so $\Delta W_{ev}=0$, and the other available materials and their properties are listed and presented in *Table 13* and in *Fig. 34.*

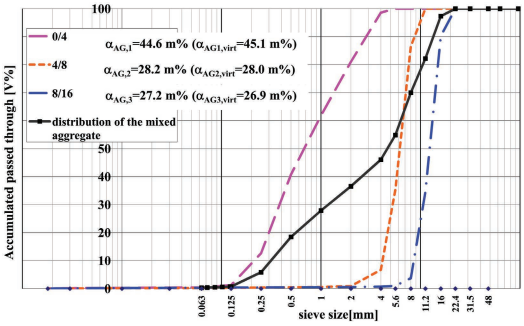

Fig. 34. Data on the particle distribution of aggregates that are available for concrete with designation C30/37-XC3-16-F4-MSZ 4798-1:2004, which is to be designed in our example.

34. ábra A példa szerint tervezendő C30/37-XC3-16-F4-MSZ 4798-1:2004 jelű betonhoz rendelkezésre álló adalékanyagok szemeloszlási adatai

6.3 Identifying the correlations related to the design criteria as target parameters

Instead of searching for new, universally valid correlations, the simple basic model for concrete mixes preferably relies on local correlations, obtained through *experience* from *controlled experimental data*, whose validity is restricted to the materials used in the given experiment and their range of interpretation. Such experimental correlations may be obtained at any concrete mixing plant where industrial production is controlled under supervision by trained professional concrete technicians.

The correlations obtained through experience are used here that relate to compressive strength and to consistency. Validity extends to the concrete constituents identified in *paragraph 6.2*. 46 observations are available for the compressive strength of mixes made from CEM II/A-M (V-LL) 42.5 N cement, and 10 observations are available for the consistence of mixes with MRWR admixture (see *Tables 14* and *15*).

For the experiential correlations used for compressive strength Eq. (33) applies, but replacing $f_{c,28}$ with $f_{cm,28,exp}$ which is the expected mean compressive strength of concrete at the age of 28 days, see Eq. (41).

$$f_{cm,28,exp} = A \cdot \frac{\chi_c^{n_\chi} \cdot p^{n_p}}{(1+x)^{n_x}} \cdot (1-l)^{n_l} \qquad (41)$$

where:

$f_{cm,28,exp}$ [N/mm²] is the target mean compressive strength measured on cube specimens after 28 days standard curing,

A is the experiment constant, for CEM II/A-M (V-LL) A=342.302,

χ_c is the cement volumetric ratio in the paste powder, n_χ is the exponent of χ_c, for CEM II/A-M (V-LL) n_χ=1.711,

p is the paste volumetric ratio in the concrete, n_p is the exponent of p, for CEM II/A-M (V-LL) n_p=-0.240,

x is the liquid-paste volume factor in the paste, n_x is the exponent of (1+x), for CEM II/A-M (V-LL) n_x= 2.355

l is the air volumetric ratio in the concrete, n_l is the exponent of l, for CEM II/A-M (V-LL) n_l= 3.75.

For the experiential correlations used for consistence Eq. (39) applies, but replacing *Flow* with $Flow_{exp}$ which is the *expected* mean flow value of the fresh concrete mix, see Eq. (42).

$$Flow_{exp}[mm] = \left(1 + f_{1,AD} \cdot \lambda_{AD}\right) \cdot f_{2,AD} \cdot A \cdot \frac{\left(\frac{x}{f_z}\right)^{n_x}}{\left(1+\frac{a \cdot f_a}{z \cdot f_z}\right)^{n_f} \cdot \left(1+\frac{a}{z}\right)^{n_a}} \qquad (42)$$

where:

$Flow_{exp}$ is the expected mean flow value [mm] of the concrete mix by flow table,

λ_{AD} is the dose of admixture in the volumetric ratio of paste powder (concrete composition content indicator),

$f_{1,AD}$ is the *dose factor* of the admixture (for specific values of MRWR see *Table 15*),

$f_{2,AD}$ is the factor typical of the *material* of the admixture (for specific values of MRWR see *Table 15*),

A is the experimental constant, in this case A=39386.8,

n_x, n_f and n_a are exponents, with observed values as follows: n_x=0.288, n_f=1.208 and n_a=0.319,

f_z is the volumetric specific surface area of the paste powder [m²/m³], in this case $f_z \approx \chi_c f_c + (1-\chi_c) f_K$, ($f_c$ and f_K according to *Table 13*),

f_a is the volumetric specific surface area of the aggregate [m²/m³], in this case f_a according to *Table 13*,

z is the volumetric ratio of paste powder in the concrete ($z=p/[1+x]$),

a is the volumetric ratio of aggregate in the concrete ($a=1-l-p$).

Finally, the correlations to be considered due to the restriction $w/c \leq 0.55$ can be given by Eq. (43).

$$x \approx \chi_c \cdot \left(\frac{w}{c} - sw_c\right)\frac{\rho_c}{\rho_f} \qquad (43)$$

where ρ_f is the mean density of the liquid constituents in the concrete (mostly water).

Substituting the data in Eq. (43) ρ_c and sw_c from *Table 13* and ρ_f=1000 kg/m³ gives Eq. (44).

$$x \leq \chi_c \cdot (0.55 - sw_c)\frac{\rho_c}{\rho_f} = \chi_c \cdot (0.55 - 0.0151)\frac{3000}{1000} = 1.6047 \cdot \chi_c \qquad (44)$$

6.4 Determining the concrete composition content indicators required to fulfil the criteria, and determining the possible mix compositions by solving the system of material balance equations

Concrete mixes are determined by *five* linearly independent content indicators, but there are *two* estimate formulae, Eqs. (41) and (42), and furthermore, one of the content indicators is assumed to have a value of l=0.020 (therefore with an air content of 20 litres/m³), so the number of concrete composition content indicators that may be freely selected is reduced to two, and even between x and χ_c there is the restriction given by Eq. (44). It is practical to freely select the values of p and χ_c, and to calculate – from the interactions of Eqs. (41), (42) and (44) – the possible content indicators x and λ_{AD}. After the five content indicators have been determined in this way, they also provide the *structural* vector

on the right hand side of Eq. (40), from which the matrix equation can be solved to find the mix composition vector. The calculations in the example have been performed for *paste contents* of 280 and 300 l/m^3 (p=0.280 and p=0.300) and for addition *contents* of *almost zero* and 15 V% (χ_c =0.850 and χ_c=0.972…0.976) and the results of the calculations are presented in *Table 16*.

6.5 Discussion

Of the mix compositions presented in *Table 16*, mixes no. 1, 6 and 7 fulfil all the requirements, including those for body density – which are too strict in the opinion of the author of the present paper. The data in *Table 16* show that there is not much to be gained by increasing the paste content in a given concrete and by targeting the *upper* limit within the strength class, as this involves an increase in the dose of cement, and furthermore the dose of water reducing admixture also needs to be increased. The mix that best meets the requirements is no. 1, in the opinion of the author of the present paper, even though mix no. 1 also has the blemish in that according to *Table 15*, the industrial observations were in the range λ_{AD} <0.030, while here one can see λ_{AD} = 0.034, which is an *extrapolated* value. It would be possible to make adjustments by amending the flow value criterion, but it is not worthwhile, as even if λ_{AD} = 0.030, the estimated flow value is ~508 mm, which is a negligible difference to the designed 520 mm.

7. Present and future tasks in concrete engineering

Concrete engineering in the last few decades has witnessed the appearance of newer and newer types of cements and admixtures, and it is impossible for standard methods to keep up with technical developments when it comes to describing the effects of the new materials. This necessitated a new systematic and harmonised examination of the effects of concrete constituents, in order to gain a deeper insight into their effects. This is not just in the interest of the cement producers or the companies that distribute the admixtures, but also in the interest of concrete mixing plants. Research is already underway in many institutes separately. Author of the present paper has no doubt about the commitment of ÉMI Nonprofit Ltd in this sense: the research is ongoing in cooperation with scientific institutions and with smaller and larger concrete mixing plants, which have the objective of optimising concrete compositions and of improving the advancement of the technical culture in concrete mixing plants.

8. Acknowledgments

The author owes his gratitude to the managers of the Augusztin Concrete Manufacturing Company and of ÉMI Nonprofit Ltd for providing the ideal circumstances for preparing this work, and to DDCM Ltd and BASF Hungary Ltd for generously providing some of the research materials. Colleagues who need to receive thanks in person are: Dr. Tamás *Bánky*, Dr. Károly *Kovács*, Dr. Károly *Matolcsy*, Mrs. Éva *Horváth Török* and Mr. Sándor *Boros* for their support and countless well-intentioned remarks. Special thanks to Mr. Ferenc *Spránitz* for his invaluable advice, to Mr. Bálint *Augusztin* Jr. and Mr. Attila *Bohák* for the especially valuable and conscientious work they did in conducting the experiments and in developing the concrete test protocol. The author is respectfully grateful to his former teachers Dr. János *Ujhelyi*, Dr. György *Balázs*, Dr. Attila *Erdélyi*, Dr. Kálmán *Szalai*, Dr. Tibor *Kausay* and many other people whose life achievements set a high standard for future generations of engineers.

References

[1] Alexanderson, J.: Design of concrete mixes. *Materials and Structures*, Vol. 4, No. 4, July, 1971. pp. 203-212. http://dx.doi.org/10.1007/BF02478946

[2] Ujhelyi, J.: A beton struktúrájának és nyomószilárdságának tervezése. Doktori értekezés. *Magyar Tudományos Akadémia* 1989. augusztus.

[3] Spránitz, F.: „Érdemes-e küszködni az NT betonokkal? 4. rész – avagy milyen neműek a nagy teljesítőképességű (NT) betonok?", *Beton*, XVII. évf. 1. szám, 2009. január, pp. 3-7.

[4] Spránitz, F.: „Érdemes-e küszködni az NT betonokkal? 5. rész - avagy milyen neműek a nagy teljesítőképességű (NT) betonok?", *Beton*, XVII. évf. 2. szám, 2009. február, pp. 3-6.

[5] Toutou, Z. – Roussel, N.: Multi Scale Experimental Study of Concrete Rheology: From Water Scale to Gravel Scale. *Materials and Structures*, Vol. 39, No. 2, March, 2006. pp. 189-199. http://dx.doi.org/10.1617/s11527-005-9047-y

[6] Pekár, Gy.: Simple basic model for concrete and its application. 2. Factors that infl uence compressive strength and drying shrinkage *Építőanyag*, 65. évf. 3. szám (2013), pp. 76–84. http://dx.doi.org/10.14382/epitoanyag-jsbcm.2013.15

[7] Kausay, T.: Beton adalékanyagok szemmegoszlási jellemzőinek számítása grafoanalitikus módon. Vasbetonépítés. VI. évf. 1. szám 2004. pp. 3-11.

[8] Pekár, Gy.: Simple basic model for concrete and its application. 1. Content indicators of concrete mixtures and mixing plant observations. *Építőanyag*, 65. évf. 2. szám (2013), pp. 52–60. http://dx.doi.org/10.14382/epitoanyag-jsbcm.2013.12

[9] MSZ EN 206-1:2002, MSZ EN 206-1:2000/A1:2004, MSZ EN 206-1:2000/A2:2005 Concrete. Part 1: Technical conditions, performance, preparation and compliance.

[10] Palotás, L. – Balázs, L.: Mérnöki szerkezetek anyagtana III. *Akadémiai Kiadó*, Budapest 1980.

[11] Arany, P. – Nehme, S. G. – Fehérvári, S.: Építőanyagok I. (BSc-BMEEOMAT12) Laboratóriumi gyakorlati segédlet. Betontervezés. *BME Építőanyagok és Mérnökgeológia Tanszék*, 2008. április 7.

Ref.:
Gyula **Pekár**: *Simple basic model for concrete and its application Part 3. Factors affecting consistency, material balance equations and mix design*
Építőanyag, 65. évf. 4. szám (2013), 118–126. p.
http://dx.doi.org/10.14382/epitoanyag-jsbcm.2013.22

Betonkeverékek egyszerűsített alapmodellje és alkalmazása
3. rész: Konzisztenciát befolyásoló tényezők, anyagmérleg egyenletek, összetételek tervezése
A gyártóüzemi megfigyelések során a konzisztenciára vonatkozóan is számos érdekes kérdés merült fel. A szerző véleménye szerint igazán értékelhető adathalmazt éppen a gyártóüzemekben (illetve a transzportbeton kiszállítási helyszínein) végzett vizsgálatokkal nyerhetünk. Mindazonáltal a statisztikai jellemzők a konzisztencia tekintetében korántsem igazolnak olyan szoros kapcsolatot, mint a szilárdság vagy az alakváltozás esetén, ezért a kellő óvatosság indokolt, bár az óvatosság sosem jelentheti azt, hogy legyintve mondjunk le bizonyos következtetések levonásáról. A betonösszetételi (strukturális) állapotjelzők bevezetése hasznos lehet a friss (és megszilárdult) betonkeverékek összetételének tervezése során is, amennyiben ismerjük, vagy kísérleti úton meghatározzuk a betonösszetételi állapotjelzők és a friss és megszilárdult beton tulajdonságai közötti összefüggéseket, és alkalmazzuk a betonkeverékek anyagmérleg egyenleteit. A cikksorozat befejező része ezeket a kérdéseket mutatja be.

Collection for Recycling rates in Europe

More than 70% of glass bottles and jars collected for recycling in the EU.
Over three quarters of them are used as secondary raw material in a resource-efficient bottle to bottle loop.
http://www.feve.org

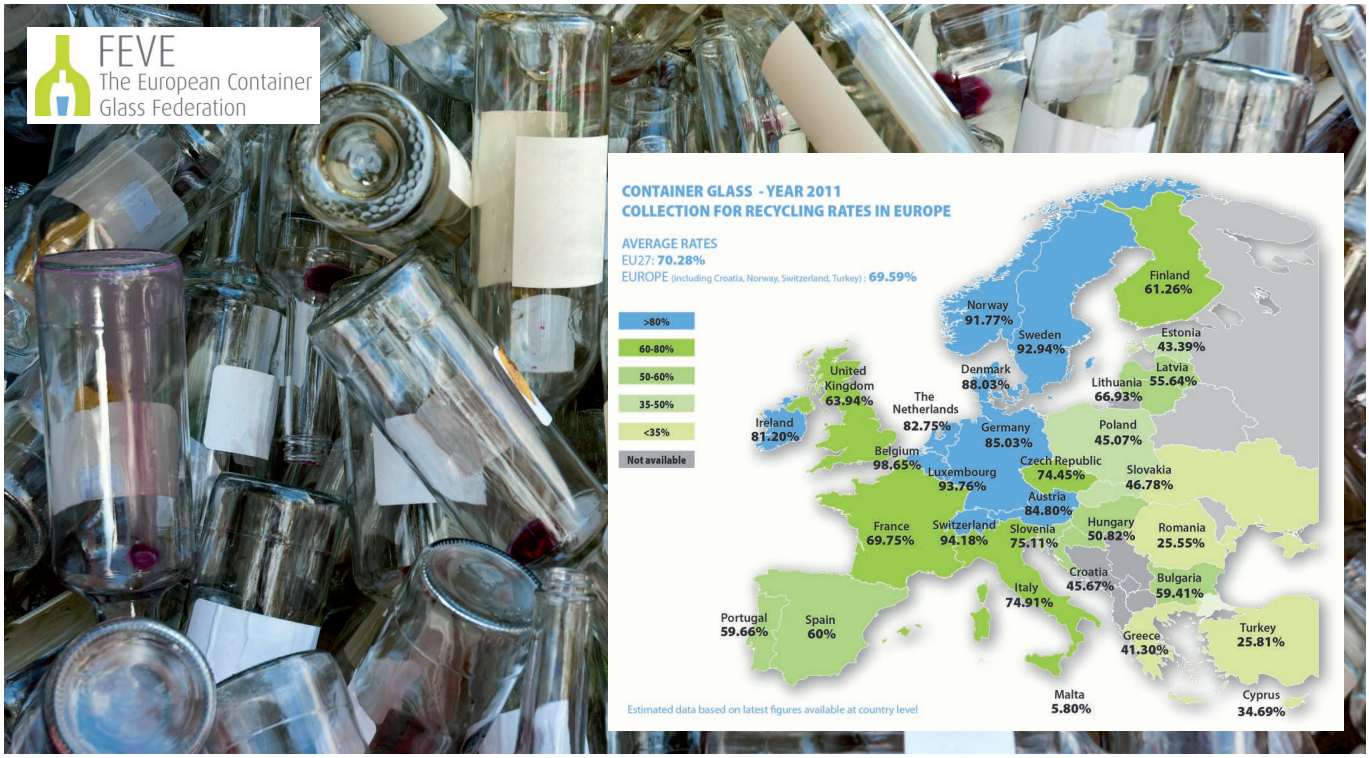

According to the latest glass recycling industry data – published on 26 March 2013 by the European Container Glass Federation (FEVE) – the average glass recycling rate in the European Union has risen above the 70% threshold for the first time. This means that over 11 million tons were collected throughout the European Union in 2011.

This achievement follows major efforts made in all EU Member States over the past few years to meet the EU's 60% recycling target for glass, a level that was reached by all the relevant countries by 2008. Some of them recorded particularly outstanding results. Other countries are in good shape to meet the target within the later fixed deadlines, while for some there is still potential to improve.

All participants in the glass closed loop have contributed to these good results. On the one hand, the glass industry has designed, manufactured and marketed containers to be effectively recycled in a closed loop system. They have also effectively communicated good recycling practices to consumers. On the other hand, collection and processing schemes have also been extended and progressively improved, while the public has also been made aware of the importance of collecting more glass and better. Used glass bottles are a precious resource and should be properly collected through separate streams.

"We have no problems in absorbing more recycled glass provided that this is of high quality. Glass recycling is the key component of the circular economy – because recycling closes the loop." says Mr. Stefan *Jaenecke*, President of FEVE - Glass recycling saves raw materials and energy and reduces production costs.

Made of natural minerals abundant in nature – sand, soda-ash and limestone – glass is a100% recyclable material, manufactured in a one step process under one roof. Each time a bottle or jar is recycled into new containers, energy and raw materials are saved and less CO_2 is emitted. Eighty per cent of glass collected for recycling is used over and over again to produce new glass bottles in the closed loop system.

By recycling glass, in 2011 in the EU:

- Over 12 million tons of raw materials (sand, soda ash, limestone) were saved.
- Over 7 million tons of CO_2 were avoided equal to taking 4 million cars off the road.
- A saving of 2,5% energy for each 10% of glass recycled in the furnace.

More needs to be done to collect the remaining 30% of used glass that currently is wasted, and to promote a circular economy that suits the ambitious vision of the European Commission to build a "zero waste" and "resource efficient" society.

"Glass is a mono-material and does not require any additional barriers to preserve food and drinks, and its infinite recycling is a unique property", says FEVE Secretary General, Ms. Adeline *Farrelly*. She adds: *"We advocate suitable legislation that acknowledges and incentivises real recycling."*

Published on **www.feve.org**.

GUIDELINE FOR AUTHORS

The manuscript must contain the followings: title; author's name, workplace, e-mail address; abstract, keywords; main text; acknowledgement (optional)**; references; figures, photos with notes; tables with notes; short biography** (information on the scientific works of the authors).

The full manuscript should not be more than 6 pages including figures, photos and tables. Settings of the word document are: 3 cm margin up and down, 2,5 cm margin left and right. Paper size: A4. Letter size 10 pt, type: Times New Roman. Lines: simple, justified.

TITLE, AUTHOR

The title of the article should be short and objective.
Under the title the name of the author(s), workplace, e-mail address.
If the text originally was a presentation or poster at a conference, it should be marked.

ABSTRACT, KEYWORDS

The abstract is a short summary of the manuscript, about a half page size. The author should give keywords to the text, which are the most important elements of the article.

MAIN TEXT

Contains: materials and experimental procedure (or something similar), results and discussion (or something similar), conclusions.

REFERENCES

References are marked with numbers, e.g. [6], and a bibliography is made by the reference's order. References should be provided together with the DOI if available.
Examples:
Journals:
[6] Mohamed, K. R. – El-Rashidy, Z. M. – Salama, A. A.: In vitro properties of nano-hydroxyapatite/chitosan biocomposites. *Ceramics International.* 37(8), December 2011, pp. 3265–3271, http://dx.doi.org/10.1016/j.ceramint.2011.05.121
Books:
[6] Mehta, P. K. – Monteiro, P. J. M.: Concrete. Microstructure, properties, and materials. *McGraw-Hill*, 2006, 659 p.

FIGURES, TABLES

All drawings, diagrams and photos are figures. The **text should contain references to all figures and tables**. This shows the place of the figure in the text. Please send all the figures in attached files, and not as a part of the text. **All figures and tables should have a title**.
Authors are asked to submit color figures by submission. Black and white figures are suggested to be avoided, however, acceptable.
The figures should be: tiff, jpg or eps files, 300 dpi at least, photos are 600 dpi at least.

BIOGRAPHY

Max. 500 character size professional biography of the author(s).

CHECKING

The editing board checks the articles and informs the authors about suggested modifications. Since the author is responsible for the content of the article, the author is not liable to accept them.

CONTACT

Please send the manuscript in electronic format to the following e-mail address: femgomze@uni-miskolc.hu and epitoanyag@szte.org.hu or by post: Scientific Society of the Silicate Industry, Budapest, Bécsi út 122–124., H-1034, HUNGARY

We kindly ask the authors to give their e-mail address and phone number on behalf of the quick conciliation.

INHALT

97 Vergleich der Sorptionseigenschaften von natürlichen und synthetischen Takoviten, $Ni_6Al_2(OH)_{16}CO_3.4H_2O$

102 Analyse von räumlichen Variabilität des Rückprallhammers während in-situ Versuche

107 Messbare Eigenschaften der Rohmaterialien Al_2O_3 vom Keramik Spritzgießen

112 Laboratorische Untersuchung des Knickens von Glassäule. Teil 2

118 Vereinfachtes Grundmodell von Betonmischungen und Anwendung. Teil 3: Konsistenz, Material Balance Gleichung und Planung der Betonmischungen

СОДЕРЖАНИЕ

97 **Природные и синтетические таковиты, сравнение сорбционных свойств $Ni_6Al_2(OH)_{16}CO_3.4H_2O$**

102 **Оценка изменчивости результатов в зонах измерения при испытаниях молотком Шмидта**

107 **Характерные параметры керамических молдинг-масс на базе**

112 **Лабораторные исследования изгиба стеклянных столбов. Часть 2**

118 **Простая базовая модель для бетонов и её применение. Часть 3. Консистенция, уравнения материального баланса, рассчет состава**

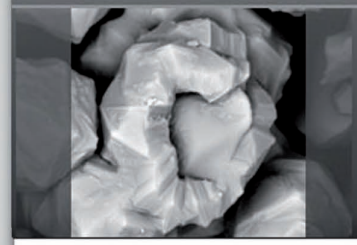

We are pleased to announce the organization of

ic-cmtp3

THE 3rd INTERNATIONAL CONFERENCE ON COMPETITIVE MATERIALS AND TECHNOLOGY PROCESSES

to be held at Hunguest Hotel Palota Lillafüred in Miskolc, Hungary, October 6-10, 2014.

The 2nd International Conference on Competitive Materials and Technology Processes was also held in this wonderful palace hotel in the exceptionally beautiful **Bükk Mountains** and together with coauthors have participated on it more than **550 scientists** from **36** countries of Asia, Europe, America and Africa.

The peer reviewed and accepted papers of **ic-cmtp3** conference will be published in periodicals of IOP Conference Series: Materials Science and Engineering (MSE) which are referred by Scopus, EI Compendex, Inspec, INIS, Chemical Abstracts, NASA Astrophysics Data System and many others. As organizers we hope you will submit your abstract and will attend on **ic-cmtp3** conference and we are looking forward to welcome you in **Miskolc, Hungary in October 6-10, 2014.**

The objectives

The event based more to academia than to industry and all papers will be peer reviewed before publication in **IOP Conference Series Materials Sciences and Engineering**, which is refereed by SCOPUS and many others. The international conference **ic-cmtp3** provides a platform among leading international scientists, researchers, engineers, students and PhD students for discussing recent achievements in research and development of material structures and properties of competitive materials like nanomaterials, ceramics, glasses, films and coatings, metals, alloys, biomaterials, composites, hetero-modulus and hybrid-materials, ... etc.

Among the major fields of interest are materials with extreme physical, chemical, thermal, mechanical properties and dynamic strengths; including their crystalline and nano-structures, phase-transformations as well as methods of their technological processes, tests and measurements.

Promote new methods and results of scientific researches and multidisciplinary applications of material science and technological problems encountered in sectors like ceramics, glasses, metal alloys, thin films, aerospace, automotive and marine industry, electronics, energy, security, safety and construction materials, chemistry, medicine, cosmetics, biosciences, environmental sciences are of particular interests.

Sessions

Session 1: Advanced Materials for Bio- and Medical Applications
Session 2: Advanced Materials for Extreme Applications
Session 3: Advanced Nanomaterials with Predesigned Properties
Session 4: Biomaterial Derived Ceramics and Composites
Session 5: Glasses, Coatings and Related Materials
Session 6: Hetero-Modulus, Hetero-Viscous and Hybrid Materials
Session 7: Light-Weight Metals and Alloys
Session 8: Materials with Extreme Dynamic Strength for Safety and Security
Session 9: Membranes and Catalysts
Session 10: Minerals for Environmental and Medical Applications
Session 11: Nanomaterials for Environment and Health
Session 12: Novel Synthesis and Processing Technology
Session 13: Phase Diagram as a Tool of Materials Science
Session 14: Polymer Derived Ceramics
Session 15: Processing and Properties of Silicate Ceramics
Session 16: Refractory and Fireproof Materials

Important Dates

Please, be so kind and keep the following important dates of the 3rd International Conference on Competitive Materials and Technology Processes ic-cmtp3:

Sessions proposal deadline	December 20th, 2013
Abstract submission deadline:	February 28th, 2014
Notification of acceptance:	March 30th, 2014
Early registration deadline:	April 30th, 2014
Early registration fee payment deadline:	May 20th, 2014
Registration fee payment deadline:	August 10th, 2014

Further information can be obtained from Prof. Dr. László A. Gömze by e-mail femgomze@uni-miskolc.hu

The Young ceramic Researchers Network (YCN) is an initiative of the European Ceramic Society (ECerS) sponsored by the JECS Trust. This nonprofit network aims at bringing young students and professionals currently doing research on Ceramics. The YCN was founded during the ECerS conference in Krakow (Poland) on June 23, 2009.

MISSION, AIMS, AND VALUES

All members share a common feature: to conduct research on the field of Ceramics.

- Promote research in the field of Ceramics
- Facilitate and encourage contacts, meetings, links between young researchers
- Facilitate the exchange of ideas, work experience, the access to some facilities, the mobility of its members in the European space
- Increase the scientific training of its members by organizing conferences, symposia, thematic schools
- Help its members find a permanent position (in academic research and/or industry) or other all around the world

http://www.young-ceramic.org

ECERS

JECS Trust